Site U1363[1]

Expedition 327 Scientists[2]

Chapter contents

Site summary 1
Background and objectives 3
Operations 3
Lithostratigraphy 5
Petrology 5
Pore water geochemistry 6
Microbiology 7
Physical properties 7
Paleomagnetism 9
Downhole measurements 9
References 10
Figures 11
Tables 26

Site summary

Five holes were cored during Integrated Ocean Drilling Program (IODP) Expedition 327 at Site U1363, adjacent to the edge of Grizzly Bare outcrop (see Tables **T1, T2, T3** and Fig. **F3B** in the "Expedition 327 summary" chapter). Sediments are composed of turbidites interspersed with hemipelagic clay, consistent with core recovery during Ocean Drilling Program (ODP) Leg 168 and IODP Expedition 301, >50 km to the north (Davis, Fisher, Firth, et al., 1997; Fisher, Urabe, Klaus, and the Expedition 301 Scientists, 2005). Four lithologic units were distinguished.

Unit 1 is composed of hemipelagic mud (clayey silt to silty clay), thin-bedded turbidites (sand-silt-clay), and thick-bedded medium sand turbidites. Unit 2 is composed of beds of silt and sandy silt intercalated with hemipelagic mud deposits (silty clay to clayey silt). Unit 3 is composed of hemipelagic carbonate-rich claystone rich in foraminifers and nannofossils. Unit 4 is represented by a few small pieces of basalt recovered from the sediment/basalt interface in Holes U1363B, U1363D, and U1363F. The basalt is cryptocrystalline and plagioclase phyric, with glomeroporphyritic texture visible in hand specimens. Phenocrysts are large (up to 8 mm) and are anhedral to euhedral in shape. The basalt is sparsely vesicular with highly variable vesicle size and shape. Secondary minerals are present as background groundmass replacement and alteration halos as well as filling vesicles and lining hydrothermal veins.

All cores were run through the Whole-Round Multisensor Logger (WRMSL), yielding magnetic susceptibility values from $<500 \times 10^{-6}$ SI in clay sections to $\sim1400 \times 10^{-6}$ SI in sandy turbidites. Point magnetic susceptibility data collected with the Section Half Multisensor Logger (SHMSL) are similar, with split-core values tending to be slightly lower than whole-round values, except in the case of turbidite sequences, where SHMSL values are consistently higher. Gamma ray attenuation (GRA) bulk density averages ~1.8 g/cm^3, depending on lithology, with some compaction evident with depth in clay intervals. *P*-wave velocities measured on the WRMSL range from ~1.46 to ~1.87 km/s, excluding the erroneously low values derived from insufficient sediment filling within core liners.

Discrete measurements, including moisture and density (MAD), *P*-wave velocity, and thermal conductivity, were measured on most cores from Holes U1363B–U1363D and U1363F. Insufficient time was available to measure samples from Hole U1363G.

[1] Expedition 327 Scientists, 2011. Site U1363. *In* Fisher, A.T., Tsuji, T., Petronotis, K., and the Expedition 327 Scientists, *Proc. IODP,* 327: Tokyo (Integrated Ocean Drilling Program Management International, Inc.). doi:10.2204/iodp.proc.327.106.2011
[2] **Expedition 327 Scientists' addresses.**

doi:10.2204/iodp.proc.327.106.2011

Thermal conductivity at Site U1363 averages 1.3 ± 0.2 W/(m·K), whereas MAD bulk densities average 1.7 g/cm^3, both showing bimodal distributions corresponding to clay and sand lithologies. MAD porosities range from 38% to 76%, with an average value of ~60%. *P*-wave velocities of discrete samples range from 1.49 to 1.75 km/s (mean = ~1.52 km/s), with considerable variability across lithologies. Velocities derived from discrete measurements agree with those measured on whole-round sections with the WRMSL. Velocities also show weak anisotropy between vertical and horizontal directions. *P*-wave velocity increases ~50 m/s within the uppermost 50 meters below seafloor (mbsf). On the other hand, grain density is remarkably consistent regardless of depth or lithology.

Pore water samples were recovered from five holes, providing systematic trends to assess the composition of the underlying basaltic formation fluid at these locations. Pore waters were extracted in a nitrogen atmosphere, and some analyses (alkalinity and ion chromatography) were conducted immediately to guide subsequent drilling operations. We collected 58 pore water samples: 15 from Hole U1363G, 14 from Hole U1363F, 14 from Hole U1363B, and 15 from (adjacent) Holes U1363C/U1363D, with basement depths of 17, 35, 57, and 231 mbsf, respectively. In the upper portion of sediment, biogenic processes release dissolved Mn and Fe near the sediment/water interface and consume sulfate. There is a corresponding increase in alkalinity, phosphate, and ammonium and an initial decrease in Ca resulting from carbonate formation. There are similar trends for sulfate, Mn, and Fe near the sediment/basalt interface. However, phosphate and ammonium are more influenced by diffusion and reaction within the upper basaltic basement. The cations Ca, Mg, and K show gradients near the sediment/basalt interface that are indicative of a formation fluid that is slightly altered relative to seawater. Minor and trace elements in seawater also show gradients in the basal sediment section, with greater alteration at greater distance from the outcrop.

Microbiologists collected whole-round core and pore water samples from sediments and basement pieces recovered at Site U1363. Eleven sediment intervals were targeted for microbiology sampling in Hole U1363B. Most samples were taken from hemipelagic clay layers, although some sandy turbidite layers were also sampled. The deepest sediment sample was taken from a carbonate-rich layer near the sediment/basalt interface. Thirteen sediment intervals and one basement basalt interval were sampled from Holes U1363C and U1363D. Again, sediment samples were mostly from clay-rich layers, although some samples contained sand. The basement sample from Core 327-U1363D-6X was a relatively unfractured basalt with spots of light green and orange alteration crusts. Nineteen sediment and basement samples were taken from Hole U1363F. Most samples contained either clay or sandy layers, with the exception of samples from Section 327-U1363F-4H-2 and deeper, which also contained manganese crust, basalt fragments, and lighter tan-colored sediment resembling the foraminifer-rich carbonate sediments from Hole U1363B. Sixteen samples were collected from Hole U1363G. All samples were clay rich, and no hard rock samples were recovered.

At each sampling location whole-round core samples were collected for shore-based DNA analysis, characterization of halogenated organic matter, and incubation experiments to examine dehalogenation reaction activities. Syringe samples were also collected for headspace gas analysis and microsphere contamination checks from the interior and exterior of the cores. Headspace samples were analyzed on board for safety purposes, and only a few samples contained quantifiable levels of methane or higher hydrocarbon gases. Microsphere samples were shipped to the shore-based laboratory for postcruise analysis because of time limitations at the end of the expedition. These samples will also be used for shore-based cell counting analysis and fluorescent in situ hybridization (FISH) analysis. A subset of samples was collected for analysis of dissolved organic carbon (DOC)/dissolved nitrogen (DN), particulate organic carbon (POC)/particulate nitrogen (PN), amino acids, low molecular weight organic acids, and lipid biomarkers.

Remanent magnetization measurements were made on two-thirds of core sections from Hole U1363B. Samples were demagnetized at 10 mT steps from 0 to 40 mT using the cryogenic magnetometer's inline alternating-field (AF) coils. Although the majority of samples have positive inclinations, there is a large scatter of positive and negative inclinations, which is probably the result of core disturbance during coring.

Temperature measurements were collected with the third-generation advanced piston corer temperature tool (APCT-3) and the Sediment Temperature (SET) tool in Holes U1363B, U1363C, U1363F, and U1363G. Good measurements were obtained with both tools, and these data will be analyzed postexpedition to assess seafloor heat flow and thermal conditions in basement.

Background and objectives

The eastern flank of the Juan de Fuca Ridge has been the target of numerous mapping, heat flow, sediment coring, seismic, drilling (Leg 168 and Expedition 301), and submersible expeditions (e.g., Davis et al., 1992; Davis, Fisher, Firth, et al., 1997; Wheat et al., 2004; Fisher, Urabe, Klaus, and the Expedition 301 Scientists, 2005; Hutnak et al., 2006). The central goal of these studies has been resolving coupled hydrogeologic, geochemical, and microbiological processes and properties within a ridge-flank hydrogeologic system where fluids, heat, and solutes are driven by lithospheric cooling and focused by areas of basement exposure. Determining rates and patterns of hydrothermal circulation in the ocean crust in this area is essential for developing a process-based understanding of how these systems work.

There are three basement outcrops located 100 km east of the active spreading center on the Juan de Fuca Ridge on 3.5–3.6 Ma seafloor and surrounded by turbidites and hemipelagic sediment that is 250–600 m thick: Papa Bare, Mama Bare, and Baby Bare (Davis et al., 1992; Underwood et al., 2005) (Fig. F1). These three outcrops are locations where altered seawater from ocean crust vents to the overlying ocean. Studies of Baby Bare outcrop suggest a total fluid discharge rate of 2–10 L/s (Wheat et al., 2004). In contrast, Grizzly Bare outcrop is a large basaltic feature 52 km to the south, where heat flow, seismic, and modeling studies indicate that cold seawater enters the crust (Fisher et al., 2003; Hutnak et al., 2006). These studies suggest a northeastern direction of fluid flow in basement from Grizzly Bare to Baby Bare outcrop, perhaps enhanced by the tectonic and structural fabric of the crust, which imparts azimuthal anisotropy in permeability (Wheat et al., 2000; Fisher et al., 2008). As at other locations where ridge-flank hydrothermal circulation is guided by basement outcrops, seawater is hypothesized to enter basaltic basement, flow laterally within the crust and become warm, react with basalt, exchange solutes with overlying pore waters in the sediment, and support microbial processes (Fisher and Wheat, 2010). Thermal and chemical changes between recharge and discharge sites are expected to be systematic, with temperatures that rise from 2° to 64°C and a fluid composition that loses dissolved oxygen, nitrate, and magnesium while gaining calcium. The time required for transition from oxic seawater to a hydrothermal fluid in this setting is not known with confidence but is likely to be tens to hundreds of years (Fisher et al., 2003; Hutnak et al., 2006).

Site U1363 (prospectus Sites GRB-1A, GRB-2A, and GRB-3A) is located adjacent to the northeastern edge of Grizzly Bare outcrop (Fig. F1) along reflection seismic Line GeoB00-170 (Fig. F2), co-located with a transect of shallow heat flow measurements oriented radially away from the outcrop (Zühlsdorff et al., 2005; Hutnak et al., 2006). If Grizzly Bare outcrop is a site of regional hydrothermal recharge, as hypothesized, fluid and microbiological composition at the base of the sediment column close to the outcrop should look much like that near the seafloor, whereas the chemical composition of pore fluids and microbiological communities from the middle of the sediment section should show the influence of diffusion and digenetic reactions as a function of depth, temperature, and distance from the outcrop.

Upper basement near Grizzly Bare outcrop is projected to be ~30°C where the sediment is ~200 m thick, only 700 m from exposed basalt, suggesting that seawater warms quickly as it enters basement and flows laterally. Laboratory experiments at low temperatures suggest that little change occurs on a timescale of a year at similar temperatures. This fluid also exchanges solutes via diffusion with overlying sediment pore water, which mainly influences elements that are highly reactive in the sediment (e.g., silica, nutrients, ammonium, sulfate, manganese, and iron). Microbial metabolic processes should also contribute to fluid alteration during lateral flow in basement.

The hypothesis that Grizzly Bare outcrop is a site of regional hydrothermal recharge was tested during Expedition 327 by collecting a transect of sediment cores from the northeastern edge of the outcrop, at locations where the sediment is ≤250 m thick. A transect of holes extending away from Grizzly Bare outcrop should show evidence for initial warming and losses of oxygen and nitrate in basement fluids. Many of the major ions should be little changed close to the outcrop, even if temperatures are elevated, because of the slow rate of reaction and the short residence time. The microbial population initially should be predominantly that found in bottom seawater. Farther from Grizzly Bare, as dissolved oxygen and nitrate are depleted, we anticipated finding a decrease in sulfate in fluids at the sediment/basalt interface as a result of diffusive loss to the overlying sediment. Additional changes were anticipated in other major and minor elements and in the microbial communities seen in sediments immediately above basement.

Operations

Transit to Grizzly Bare outcrop

The R/V *JOIDES Resolution* departed Site U1362 at 1300 h on 30 August 2010 following installation of a

second subseafloor borehole observatory ("CORK") at that site. The 31 nmi transit to Grizzly Bare outcrop took 3 h at an average speed of 10.0 kt. Upon arrival, the thrusters and hydrophones were lowered and the ship was moved in dynamic positioning (DP) mode to a location midway between the three projected Grizzly Bare holes so that a positioning beacon could be deployed.

Hole U1363A

At 1730 h on 30 August the ship was offset to Hole U1363A (prospectus Site GRB-1A). The sole purpose of drilling Hole U1363A was to determine the depth of basement to avoid impact with an advanced piston corer (APC) core barrel or temperature shoe at the next hole. A two-stand APC/extended core barrel (XCB) bottom-hole assembly (BHA) was made up and tripped to the seafloor, and an XCB center bit was deployed. The seafloor was tagged at 2250 h on 30 August at 2689 meters below rig floor (mbrf). Drilling without coring continued for 2.5 h to the basement contact at 58 mbsf (Table T1). The XCB center bit was recovered, and the drill string was pulled out of the seafloor.

Hole U1363B coring and temperature measurements

The ship was offset 10 m on a bearing of 135°, and Hole U1363B was spudded at 0530 h on 31 August at 2690 m. Cores 327-U1363B-1H through 6H advanced to 42.5 mbsf by 1300 h, at which point the APC was unable to penetrate the sandy turbidite formation. APCT-3 measurements were taken with Cores 3H through 6H. Cores 7X and 8X advanced to 55.0 mbsf by 1610 h. The first SET tool measurement was taken at ~56 mbsf, and coring continued with Core 9X, which advanced through the sediment/basalt interface to 57 mbsf. Core 10X advanced to 61 mbsf and was on deck by 2100 h. The drill string was pulled clear of the seafloor at 2140 h on 31 August.

Hole U1363C coring and temperature measurements

The ship was offset in DP mode to the coordinates for Hole U1363C (prospectus Site GRB-3A), the deepest of the five-hole transect at Grizzly Bare outcrop. Hole U1363C was spudded at 2255 h on 31 August at 2689 mbrf. Hole U1363C was drilled without recovering cores to 170 mbsf. A SET temperature measurement was taken at ~171 mbsf, followed by Cores 327-U1363C-2X and 3X to a depth of 183.2 mbsf. A second SET temperature measurement was taken at ~184 mbsf, followed by Cores 4X and 5X to a depth of 202.4 mbsf. A third SET temperature measurement was taken at ~204 mbsf. At 1445 h on 1 September the SET tool became stuck inside the outer core barrel because of the sandy formation, and the drill string had to be recovered back to the ship. The SET tool was retrieved at 0145 h on 2 September, and the ship was offset 10 m on a bearing of 135°.

Hole U1363D coring

Hole U1363D was spudded at 0745 h on 2 September at 2689 mbrf. Drilling without coring continued using an XCB bit to 198 mbsf. Cores 327-U1363D-2X through 5X advanced to 231 mbsf, the sediment/basalt interface, by 0035 h on 3 September, and the drill string was pulled out of the seafloor at 0700 h, ending Hole U1363D.

Hole U1363E

Hole U1363E was positioned closer to Grizzly Bare outcrop than Holes U1363A and U1363B (within the area approved for prospectus Site GRB-1A) to recover sediments and pore fluids that were less reacted. Hole U1363E was spudded at 0840 h on 3 September and was drilled without coring to determine the depth to basement. The sediment/basalt interface was confirmed at 36 mbsf at 1000 h. The drill string was pulled out of the seafloor at 1125 h, ending Hole U1363E, and the ship was offset 10 m on a bearing of 135°.

Hole U1363F coring and temperature measurements

Hole U1363F was spudded at 1200 h on 3 September, and Cores 327-U1363F-1H through 4H advanced to 35 mbsf by 1600 h. APCT-3 temperature measurements were taken with Cores 3H and 4H. The drill string was pulled out of the seafloor at 1735 h, ending Hole U1363F.

Hole U1363G coring and temperature measurements

The ship was offset even closer to Grizzly Bare outcrop (but still within the clearance area of prospectus Site GRB-1A), and basement contact was established at 17 mbsf by washing down (no hole number was assigned). Hole U1363G was spudded at 2000 h on 3 September, and Cores 327-U1363G-1H through 3H advanced to 24.9 mbsf by 2250 h. The true advance is closer to 17 mbsf because the last core recovered mostly flow-in material. An APCT-3 temperature measurement was taken with Core 2H.

Transit to Victoria, British Columbia (Canada)

The rig floor was secured for transit, and the thrusters were raised at 0930 h on 4 September. The *JOIDES Resolution* was under way at full speed at 1015 h. The pilot boarded at 0752 h on 5 September, and the first line ashore at Ogden Point, Victoria (Canada), was at 0836 h.

Lithostratigraphy

Note: This section was contributed by Sarah-Jane Jackett (Integrated Ocean Drilling Program, Texas A&M University, 1000 Discovery Drive, College Station TX 77845, USA).

Five holes were cored at Site U1363 in the vicinity of the Grizzly Bare outcrop. Four lithostratigraphic units were recognized (Fig. F3).

Unit 1 is composed of hemipelagic mud (clayey silt to silty clay), thin-bedded turbidites (sand-silt-clay), and thick-bedded medium sand turbidites. The hemipelagic mud is generally homogeneous, with local clay-rich color bands and zones of bioturbation. The mud increases in carbonate component downhole, especially calcareous nannofossils. Turbidite characteristics include sharp and erosional bases, which regularly contain a high percentage of foraminifers, normal/fining-upward grading sequences, color banding, and gradational tops. Beds of clayey silt to silty clay are generally <10 cm in thickness, whereas sand beds have a maximum thickness of 1–5 m. Medium-grained sand flow-in at the base of APC cores is common.

Unit 2 is composed of beds of silt and sandy silt intercalated with hemipelagic mud deposits (silty clay to clayey silt). Silt beds range from 1 to 5 cm in thickness, with sharp bases, normal/fining-upward grading, and gradational tops. Characteristic features include silt and fine sandy-silt laminae, slightly darker clay-rich bands, and carbonate-rich mud with foraminifers. This unit has a higher percentage of mottling from bioturbation relative to Units 1 and 3. Beds assigned to Unit 2 were probably deposited by thin, fine-grained turbidity currents. As with Unit 1, flow-in at the base of APC cores is common.

Unit 3 is composed of hemipelagic carbonate-rich claystone rich in foraminifers and nannofossils. This unit displays some brown color variations that probably were imparted by low-temperature alteration with underlying crustal rocks.

Unit 4 represents the basement at Site U1363 (see "Petrology"). Depths to basement in all holes at Site U1363 are summarized in Table T2 on the basis of a combination of core recovery and "tagged" depths identified by the driller.

Reflectance spectroscopy and colorimetry data were collected with the SHMSL to provide a high-resolution record of color variations. These data are displayed in the Site U1363 visual core descriptions in "Core descriptions."

Petrology

Basalt recovery near Grizzly Bare outcrop

Recovery of basalt from the upper ocean crust near Grizzly Bare outcrop occurred during XCB coring in Holes U1363B and U1363D but also occurred in Hole U1363F during APC coring. Basalt at Site U1363 was designated as lithologic Unit 4 (see "Lithostratigraphy"). Although only a few basalt samples were recovered, this material provides an opportunity to assess the extent of crustal alteration and microbiological activity associated with the upper crust near an area of hypothesized hydrothermal recharge.

Hole U1363B

A single 9 cm long piece of basement was recovered in Core 327-U1363B-10X. This piece is a highly clinopyroxene plagioclase phyric cryptocrystalline basalt with glomeroporphyritic texture visible in hand specimen. Phenocrysts are large (up to 8 mm) and are anhedral to euhedral in shape. The basalt is sparsely vesicular, with highly variable vesicle size and shape. Secondary minerals replace background groundmass, form alteration halos, fill vesicles, and line hydrothermal veins. Background alteration is characterized by a pale gray color, and alteration halos are dark gray and flank the hydrothermal vein and occur along the edge of the piece. Vesicle filling is variable and includes saponite or celadonite lining vesicles, completely carbonate filled to iron oxyhydroxide filled within the alteration halos and euhedral open-space, filling crystals within the larger irregular vesicles. Within this piece a 0.2 mm saponite vein network forms a mosaic-like texture in the background alteration. Down the center of the piece is a single 1 mm mixed-saponite vein lined with clay with an iron oxyhydroxide core and a 2 mm dark gray halo. This piece is interpreted to be part of a basalt pillow.

Hole U1363D

One large 6.9 cm piece taken for microbiology and three rubble chips (3.0–3.5 cm in size) were recovered from Core 327-U1363D-6X. Rubble chips are sparsely plagioclase phyric cryptocrystalline basalt.

Small millimeter-sized chilled margins are present on two of the chips. Iron oxyhydroxide and green clay occur as a patchy coating on several exterior surfaces on all three pieces.

Hole U1363F

One 1 cm piece taken for microbiology and numerous rubble chips (1–20 mm in size) were recovered from Core 327-U1363F-4H. These rubble chips are a mixture of highly plagioclase phyric glassy basalt with a manganese crust, fragments of manganese crust, and sedimentary material. Plagioclase phenocrysts are up to 3 mm in size. In some pieces an iron oxyhydroxide vein is present at the interface between the basalt and manganese crust.

Pore water geochemistry

The goal of the pore water program at Site U1363 was to recover basal sediments for pore water extraction to document trends in fluid composition with distance from the exposed basaltic portion of Grizzly Bare outcrop. Pore waters were recovered from five holes at four locations. Some analyses (alkalinity and ion chromatography) were conducted immediately to guide drilling operations. Fifty-eight pore water samples were collected: 15 from Hole U1363G, 14 from Hole U1363F, 14 from Hole U1363B, and 15 from Holes U1363C/U1363D. Basement depths are 17, 35, 57, and 231 mbsf, respectively, at these locations, as shown in Table T2 and Figures F2 and F3.

Pore water chemical profiles from three of the holes (U1363B, U1363F, and U1363G) are similar (Tables T3, T4). Results from Hole U1363B are described in the rest of this section. The upper portion of Hole U1363B was cored with the APC. Because Cores 327-U1363B-3H through 6H were partial strokes and sandy conditions caused poor recovery and sediment flow-in, the XCB was used for Cores 7X through 10X. Material from Cores 1H through 8X, with the exception of Core 6H, was squeezed to extract pore waters. Pore water profiles are similar in many ways to those from ODP Site 1026 and IODP Site U1301. In the upper portion of the sediment column, biogenic processes release dissolved Mn and Fe near the sediment/water interface and consume sulfate, with a sulfate minimum of 20.9 mM at 20.95 mbsf. There is a corresponding increase in alkalinity (Fig. F4), phosphate, and ammonium and an initial decrease in Ca resulting from carbonate formation from biogenic reactions that generate alkalinity. There are similar trends for sulfate, Mn, and Fe near the sediment/basalt interface; however, phosphate and ammonium are more influenced by diffusion and reaction within the upper basaltic basement. The gradients of cations Ca, Mg, and K near the sediment/basalt interface are indicative of a formation fluid that is slightly altered relative to seawater. Minor and trace elements in seawater also show reaction within the sediment and gradients in the basal sediment section that project to a formation fluid that is slightly altered relative to seawater.

Pore water profiles from Holes U1363F and U1363G, where the sediment section is considerably thinner, generally follow trends observed in Hole U1363B. Surprisingly, the fluid composition near the sediment/basalt interface is similar at these three locations, even though the holes are at different distances from the outcrop and have different amounts of sediment cover above basement (Figs. F2, F3). Sulfate, chlorinity, Li, and Sr concentrations differ significantly among the holes.

Only the lower portion of the sediment section was cored in Holes U1363C and U1363D. Nevertheless, spatial trends in pore water composition near the sediment/basalt interface are consistent when one considers the large-scale flow system. The composition of pore fluid at the base of Hole U1363D is more altered relative to seawater than it is in the three shallower holes discussed above (Holes U1363B, U1363F, and U1363G) but is less altered than spring fluids sampled on Baby Bare outcrop (Wheat and Mottl, 2000). An example of data quality and trends near the sediment/basalt interface is shown using alkalinity data (Fig. F4). Alkalinity concentrations increase with depth to a maximum value and then decrease in proximity to the sediment/basalt interface.

In Hole U1363G, which was APC cored to basement, alkalinity increases from 3.31 mM/L at 1.45 mbsf to 4.61 mM/L at 7.95 mbsf and then decreases to ~2.9 mM/L at a curatorial depth of 24.6 mbsf, which is 7 m deeper than the sediment/basalt contact determined by tagging basement in an unnumbered adjacent hole. Thus, fluids from a curatorial depth greater than 17 mbsf in Hole U1363G likely originated from material that was sucked into the liner during recovery of the APC core. Hole U1363F, which was XCB cored through the sediment/basalt interface, has a similar alkalinity profile (Fig. F4). In this hole, alkalinity rises from 6.65 mM/L at 4.45 mbsf to 10.5 mM/L at 12.45 mbsf and then decreases to 1.81 mM/L near the sediment/basalt interface at 33 mbsf. The highest alkalinity measured during Expedition 327 is 13.9 mM/L at 16.45 mbsf in Hole U1363B; alkalinity at the sediment/basalt interface is ~2.1 mM/L. We lack pore fluid data from the upper sediment portion of Holes U1363C and U1363D, but deeper data indicate a linear trend in composition with depth approaching the sediment/basalt interface. The lowest alkalinity measured within these

holes is 1.25 mM/L at 222.65 mbsf, near the sediment/basalt interface, which is consistent with a progressively altered basement fluid with increasing distance from Grizzly Bare outcrop. Third-party shore-based geochemistry data are included in Tables T3 and T4, and these data will be available in LIMS just like analyses that are typically run on the ship.

Microbiology

Microbiologists collected whole-round core and sediment pore water samples from sediments and pieces of hard rock basement from five holes at Site U1363. Eleven sediment depths were sampled for microbiology in Hole U1363B. Most samples were taken from clay/mud layers, although some sandy turbidite layers were also sampled. The deepest sediment sample was taken from a carbonate-rich layer near the sediment/basalt interface. Thirteen sediment depths and one basement basalt were sampled from Holes U1363C and U1363D. Again, sediment samples were mostly from clay-rich layers, although some samples contain sand. The basement sample from Core 327-U1363D-6X is relatively unfractured basalt with spots of light green and orange alteration crusts. Nineteen sediment and basement samples were taken from Hole U1363F. Most samples contain either clay or sandy layers, with the exception of samples from Section 327-U1363F-4H-2 and deeper, which also contain manganese crusts, basalt fragments, and lighter tan-colored sediment resembling foraminifer-rich carbonate sediments from Hole U1363B. Sixteen samples were collected from Hole U1363G. All samples are clay rich, and no hard rock samples were recovered in this hole.

At each sampling location, whole-round core samples were collected for shore-based DNA analysis, shore-based characterization of halogenated organic matter, and shore-based incubation experiments to examine dehalogenation reaction activities. Syringe samples also were collected for headspace gas analysis and microsphere contamination checks from the interior and exterior of the cores. Headspace samples were analyzed on board; only a few samples had quantifiable levels of methane or higher hydrocarbon gases, as anticipated for sediments in which there is still considerable sulfate in pore fluids. Microsphere samples were returned to a shore-based laboratory for postcruise analysis because of time limitations at the end of the cruise. These samples will be used for shore-based cell counting analysis and FISH analysis. A subset of samples was collected for analysis of DOC/DN, POC/PN, amino acids, low molecular weight organic acids, and lipid biomarkers.

Microsphere contamination tests

All sediment core sections sampled for microbiological analysis were sampled for microsphere contamination testing. Sterile cut-end 3 mL plastic syringes were inserted into the interior (center) and exterior (next to core liner) portions of freshly cut core sections, and sediment of a known volume was immediately fixed on the catwalk with 10 mL of cold 3.73% paraformaldehyde in 1× phosphate-buffered saline (PBS) buffer. Samples were stored cold until analysis in a shore-based laboratory. Aliquots of the homogenized sample were filtered onto 25 mm diameter, 0.2 µm mesh polycarbonate filters. Filters were examined under 100–400× total magnification with epifluorescence microscopy to quantify the number of fluorescent microspheres per sample.

Samples from Site U1363 had variable amounts of microsphere contamination (Tables T5, T6, T7, T8). None of the samples from Hole U1363B had any microspheres (Table T5). A majority of samples from the deeper sediment in Holes U1363C and U1363D were also microsphere free, with the exception of three samples (two exterior and one interior) from the deepest sediment depths near the sediment/basalt interface (Table T6). Many of the sandy sediment layers from Hole U1363F had microsphere contamination in the exterior samples, whereas the interiors were less contaminated (Table T7). In addition, the deepest sample from this hole, taken near the sediment/basalt interface, and the two shallowest samples also had microsphere contamination. Six of the sediment layers sampled in Hole U1363G, concentrated in Cores 327-U1363G-1H (sandy) and 3H (clay rich), exhibited microsphere contamination (Table T8). Much of Core 327-U1363G-3H shows evidence for flow-in (see "Operations" and "Lithostratigraphy"), which likely contributed to microsphere contamination below ~17 mbsf (depth of basement, as determined by drilling).

Physical properties

The uppermost sediment section in Holes U1363B, U1363F, and U1363G was cored using the APC. The XCB was used to core deeper sediments and the sediment/basalt interface in Holes U1363B and U1363F, as well as in Holes U1363C and U1363D.

Physical property measurements included whole-round magnetic susceptibility, density, and *P*-wave velocity and discrete measurements of thermal conductivity, *P*-wave velocity, and MAD properties (e.g., bulk density, grain density, and porosity) (Figs. F5,

F6; Table T9). Sampling frequency for the discrete samples was ~1–2 per section, taken at the same locations as thermal conductivity measurements, except in cases of fluidized sandy sections where it was not possible to extract discrete samples.

Magnetic susceptibility

All cores were run through the WRMSL, with measurements made every 2 cm (1 cm for Holes U1363F and U1363G). Magnetic susceptibility values are as high as ~1400 × 10^{-6} SI, with the highest values corresponding to sandy turbidite sequences (e.g., Cores 327-U1363B-3H and 4H) and ash layers present near the top of Core 327-U1363B-2H (Fig. F5A). Additionally, Core 327-U1363B-8X has some high magnetic susceptibility values (~1000 × 10^{-6} SI) because of the presence of iron oxides close to the sediment/basalt interface. Other cores, including clays and fine turbidite sections toward the top and bottom of the hole, generally have values of <500 × 10^{-6} SI.

After the whole-round sections were split, the archive halves were run through the SHMSL. Point measurements were made at 1 cm intervals. Magnetic susceptibility trends determined through this method are similar to those obtained from the WRMSL (Fig. F5A), with values tending to be slightly lower than those determined by the WRMSL, except in the case of turbidite sequences, where SHMSL values are consistently higher.

Gamma ray attenuation bulk density

Bulk density is estimated by GRA density measured on the WRMSL (Fig. F5B). In general, density increases slowly downhole in the uppermost 15 m, below which it varies between ~1.8 and ~2.0 g/cm^3 as a result of alternating sand and clay layers. The highest density values (~2.0 g/cm^3) occur in the massive sandy turbidites. However, because of flow-in that commonly occurs during APC coring in unlithified sands (particularly if the corer does not stroke out completely during penetration), it is unclear if these higher density values are accurate. Near the bottom of the hole (e.g., Cores 327-U1363B-8X and 9X), average GRA bulk density decreases slightly as a result of a higher clay fraction.

Thermal conductivity

A total of 153 individual measurements were made at 26 locations, yielding values averaging 1.30 ± 0.20 W/(m·K). Individual thermal conductivity measurements are typically filtered for outliers that commonly occur with the needle-probe method. Filtered data are then averaged to produce a single value. The record is most complete in sections cored with the APC because XCB cores are often too disturbed to produce reliable measurements (Fig. F6; Table T9). In general, measurements were taken at a frequency of ~1 per section, with a minimum of three measurements per location. Samples were chosen on the basis of lithology, targeting sand and clay end-members identified from maxima and minima found in WRMSL magnetic susceptibility and GRA bulk density data. The average thermal conductivity value for this site may be slightly biased toward the clay end-member because flow-in was common in sand units cored with the APC, making thermal conductivity difficult to measure. In some cases, especially shallow cores, sections were too fluidized to produce usable data because of induced fluid convection in the material during measurement. Despite these issues, the data compare well with those collected at similar depths from nearby Hole U1301C (Expedition 301 Scientists, 2005). Thermal conductivity values are inversely correlated with MAD porosity (Fig. F7A).

P-wave velocity

In addition to continuous *P*-wave velocity measurements made on whole-round sections with the *P*-wave logger (PWL), 130 measurements of *P*-wave velocity were made on split sections using the *P*-wave bayonets (PWB) or *P*-wave caliper (PWC). Because the PWC was unstable, as described in "Physical properties" in the "Site U1362" chapter, we mainly used the PWB (*y*- and *z*-axes) on section halves. For lithified sediments, however, we used the PWC (*x*-axis) because the cracks induced by the *y*- and *z*-axis transducers (bayonets) on the PWB precluded the acquisition of reliable velocities.

P-wave velocity measured with the PWL ranges from 1.46 to 1.87 km/s, with an average of ~1.57 km/s (Fig. F6A), excluding the erroneously low values derived from insufficient sediment filling within core liners. *P*-wave velocity determined by the PWB and PWC ranges from 1.49 to 1.75 km/s, with an average of ~1.52 km/s (Fig. F6A). Velocities measured in clay lithologies consistently display less variability than those measured in sand and also display a systematic increase with depth as a result of compaction. Because of mobilization and redeposition of sand layers in turbidite sequences during coring, we could not determine a statistically significant trend with depth for the sandy units.

Comparing measurements made along horizontal and vertical axes provides evidence for weak velocity anisotropy (Fig. F8). This tendency is consistent with the layered nature of these sediments and may result in part from greater clay compaction with depth.

Moisture and density

Eighty-eight discrete samples collected from Site U1363 were used to determine MAD properties (Figs. F5, F6C). Bulk density values range from 1.4 to 2.1 g/cm^3, with an average of 1.7 g/cm^3. Grain density exhibits a range of 2.7–3.0 g/cm^3, with a mean of 2.8 g/cm^3. Porosity values range from 38% to 76%, with a mean of 60%. GRA and MAD densities differ by as much as 7%. Results from Site U1362 (basement section) show that GRA results provide a lower bound on bulk density because of cores partially filling the liner, but the results derived from the sedimentary section at Site U1363 show MAD data that tend to be low relative to GRA results (Fig. F5B). This may be the case because flow-in and resedimentation of coarse material tend to cause bias in the GRA data that is avoided through more careful sample selection for MAD measurements.

P-wave velocity and porosity are clearly inversely correlated, and *P*-wave velocity and bulk density are positively correlated (Fig. F9). Sections rich in sand tend to have a high and variable *P*-wave velocity across a narrow range of porosities (V_P = 1.55–1.75 km/s for porosity = 45%–60%).

MAD data are highly variable over small depth ranges because samples were selected from the same locations as thermal conductivity measurements, which targeted end-member clay and sand lithologies. Cross-plots of bulk density and porosity show a clear linear trend, which is consistent with the method used to determine porosity, based on measured bulk and grain densities (Fig. F7B).

Paleomagnetism

Several factors limit the usefulness of the paleomagnetic analyses at Site U1363. Hole U1363B was APC/XCB cored from the surface to just below the sediment/basalt interface at 58 mbsf, recovering a sequence of hemipelagic mud and turbidite deposits (see "Lithostratigraphy"). We did not deploy nonmagnetic core barrels because of the challenging coring conditions, and cores were not oriented. During coring, sandy layers were liquefied and redeposited in the core liner. As a result, only about two-thirds of the Hole U1363B archive-half core sections were measured. Sections were demagnetized using the superconducting cryogenic magnetometer's AF coils at 10, 20, 30, and 40 mT steps and measured at 5 cm intervals. Cores from the remaining holes at this site were not measured because of time limitations.

Figure F10 displays intensity and inclination values versus depth. Some inclination values are steep, which is typical of cores that have a coring-induced overprint (Acton et al., 2002). Scattered negative inclinations or inclinations near zero are likely caused by internal core deformation rather than representing field reversals.

Downhole measurements

Determining heat flow through the sediment column and estimating uppermost basement temperatures were important operational goals at Site U1363. Sediment temperature measurements were attempted at numerous depths during sediment coring at Site U1363 using the APCT-3 and SET tools. The records will require careful processing to estimate in situ temperatures by fitting the data to decay curves for the frictional heating pulse on penetration, based on the thermal properties of the sediments, and to assess data quality and reliability. However, time did not allow for that processing to be completed during Expedition 327. Here we present only the original records of temperature versus time, with a qualitative indication of the quality of the data based on visual inspection and brief shipboard attempts to fit the data to reasonable decay curves.

It is not possible to determine if the data are of high enough quality for reliable interpretation based on a simple presentation of the temperature versus time record (as shown with figures in this chapter). Instead, the data must be processed using a range of possible sediment properties (constrained by physical property measurements, lithostratigraphic information, and core information from other sites) and different parts of the record from each deployment to assess the reliability of the results. The consistency between successive deployments in the same hole will also be assessed as part of postexpedition research.

In Hole U1363B, four deployments were made with the APCT-3 for Cores 327-U1363B-3H through 6H, but it appears that acceptable data were collected only during the deployments for Cores 3H and 5H at 21.5 and 40.5 mbsf, respectively (Fig. F11). The deployments during Cores 4H and 6H appeared to be affected by probe motion during measurement and associated movement of cool bottom water around the coring shoe (Fig. F12). Cores 4H through 6H were partial strokes because of difficulty in penetrating sandy turbidites. APC coring was suspended after Core 6H. A single deployment of the SET tool was attempted in Hole U1363B after Core 8X, but this deployment also showed evidence of probe motion when in the sediment, and measured temperatures were close to bottom water values (Fig. F13).

APC coring was not attempted in Hole U1363C, but the SET tool was deployed three times deep in the

section. The first deployment before Core 327-U1363C-2X showed evidence of probe motion (Fig. F13), but the two deployments before Cores 3X and 5X appear to have provided reliable data at ~184 and 203 mbsf, respectively (Fig. F14). These measurements suggest that temperatures in uppermost basement in Hole U1363C are close to 30°C, as estimated from surface heat flow data (Hutnak et al., 2006).

During the final day of operations, three deployments were made with the APCT-3 in Holes U1363F and U1363G, both located very close to Grizzly Bare outcrop, where the sediment cover was <40 m. Two deployments were made on Cores 327-U1363F-3H and 4H at 28.5 and 35.0 mbsf; both returned reasonable data, but the second was of better quality and indicated a basement temperature of ~7°C (Fig. F15). In Hole U1363G, the single deployment on Core 327-U1363G-2H at 16.0 mbsf yielded good data, also suggesting a basement temperature close to 7°C.

References

Acton, G.D., Okada, M., Clement, B.M., Lund, S.P., and Williams, T., 2002. Paleomagnetic overprints in ocean sediment cores and their relationship to shear deformation caused by piston coring. *J. Geophys. Res., [Solid Earth],* 107(B4):2067–2081. **doi:10.1029/2001JB000518**

Davis, E.E., Chapman, D.S., Mottl, M.J., Bentkowski, W.J., Dadey, K., Forster, C., Harris, R., Nagihara, S., Rohr, K., Wheat, G., and Whiticar, M., 1992. FlankFlux: an experiment to study the nature of hydrothermal circulation in young oceanic crust. *Can. J. Earth Sci.,* 29(5):925–952.

Davis, E.E., Fisher, A.T., Firth, J.V., et al., 1997. *Proc. ODP, Init. Repts.,* 168: College Station, TX (Ocean Drilling Program). **doi:10.2973/odp.proc.ir.168.1997**

Expedition 301 Scientists, 2005. Site U1301. *In* Fisher, A.T., Urabe, T., Klaus, A., and the Expedition 301 Scientists, *Proc. IODP,* 301: College Station, TX (Integrated Ocean Drilling Program Management International, Inc.). **doi:10.2204/iodp.proc.301.106.2005**

Fisher, A.T., Davis, E.E., and Becker, K., 2008. Borehole-to-borehole hydrologic response across 2.4 km in the upper oceanic crust: implications for crustal-scale properties. *J. Geophys. Res., [Solid Earth],* 113(B7):B07106. **doi:10.1029/2007JB005447**

Fisher, A.T., Davis, E.E., Hutnak, M., Spiess, V., Zühlsdorff, L., Cherkaoui, A., Christiansen, L., Edwards, K., Macdonald, R., Villinger, H., Mottl, M.J., Wheat, C.G., and Becker, K., 2003. Hydrothermal recharge and discharge across 50 km guided by seamounts on a young ridge flank. *Nature (London, U. K.),* 421(6923):618–621. **doi:10.1038/nature01352**

Fisher, A.T., Urabe, T., Klaus, A., and the Expedition 301 Scientists, 2005. *Proc. IODP,* 301: College Station, TX (Integrated Ocean Drilling Program Management International, Inc.). **doi:10.2204/iodp.proc.301.2005**

Fisher, A.T., and Wheat, C.G., 2010. Seamounts as conduits for massive fluid, heat, and solute fluxes on ridge flanks. *Oceanography,* 23(1):74–87. **http://www.tos.org/oceanography/issues/issue_archive/issue_pdfs/23_1/23-1_fisher.pdf**

Hutnak, M., Fisher, A.T., Zühlsdorff, L., Spiess, V., Stauffer, P.H., and Gable, C.W., 2006. Hydrothermal recharge and discharge guided by basement outcrops on 0.7–3.6 Ma seafloor east of the Juan de Fuca Ridge: observations and numerical models. *Geochem., Geophys., Geosyst.,* 7(7):Q07O02. **doi:10.1029/2006GC001242**

Underwood, M.B., Hoke, K.D., Fisher, A.T., Davis, E.E., Giambalvo, E., Zühlsdorff, L., and Spinelli, G.A., 2005. Provenance, stratigraphic architecture, and hydrogeologic influence of turbidites on the mid-ocean ridge flank of northwestern Cascadia Basin, Pacific Ocean. *J. Sediment. Res.,* 75(1):149–164. **doi:10.2110/jsr.2005.012**

Wheat, C.G., Elderfield, H., Mottl, M.J., and Monnin, C., 2000. Chemical composition of basement fluids within an oceanic ridge flank: implications for along-strike and across-strike hydrothermal circulation. *J. Geophys. Res., [Solid Earth],* 105(B6):13437–13447. **doi:10.1029/2000JB900070**

Wheat, C.G., and Mottl, M.J., 2000. Composition of pore and spring waters from Baby Bare: global implications of geochemical fluxes from a ridge flank hydrothermal system. *Geochim. Cosmochim. Acta,* 64(4):629–642. **doi:10.1016/S0016-7037(99)00347-6**

Wheat, C.G., Mottl, M.J., Fisher, A.T., Kadko, D., Davis, E.E., and Baker, E., 2004. Heat flow through a basaltic outcrop on a sedimented young ridge flank. *Geochem., Geophys., Geosyst.,* 5(12):Q12006. **doi:10.1029/2004GC000700**

Zühlsdorff, L., Hutnak, M., Fisher, A.T., Spiess, V., Davis, E.E., Nedimovic, M., Carbotte, S., Villinger, H., and Becker, K., 2005. Site surveys related to IODP Expedition 301: ImageFlux (SO149) and RetroFlux (TN116) expeditions and earlier studies. *In* Fisher, A.T., Urabe, T., Klaus, A., and the Expedition 301 Scientists, *Proc. IODP,* 301: College Station, TX (Integrated Ocean Drilling Program Management International, Inc.). **doi:10.2204/iodp.proc.301.102.2005**

Publication: 5 September 2011
MS 327-106

Figure F1. Site maps showing location of Site U1363. **A.** Regional bathymetry (Fisher et al., 2003; Hutnak et al., 2006) showing locations of ODP and IODP drill sites. Area of dashed box is shown in B. Site U1363 is located near the center of a major distributary channel for turbidites that flowed off the North American continental shelf (Davis et al., 1992; Zühlsdorff et al., 2005; Underwood et al., 2005; Hutnak et al., 2006). **B.** Bathymetry around Grizzly Bare outcrop. Black lines indicate tracks of reflection seismic lines around Site U1363 collected during the 2000 ImageFlux expedition (Zühlsdorff et al., 2005; Hutnak et al., 2006). Part of Line GeoB00-170 (red line) is shown in Figure F2.

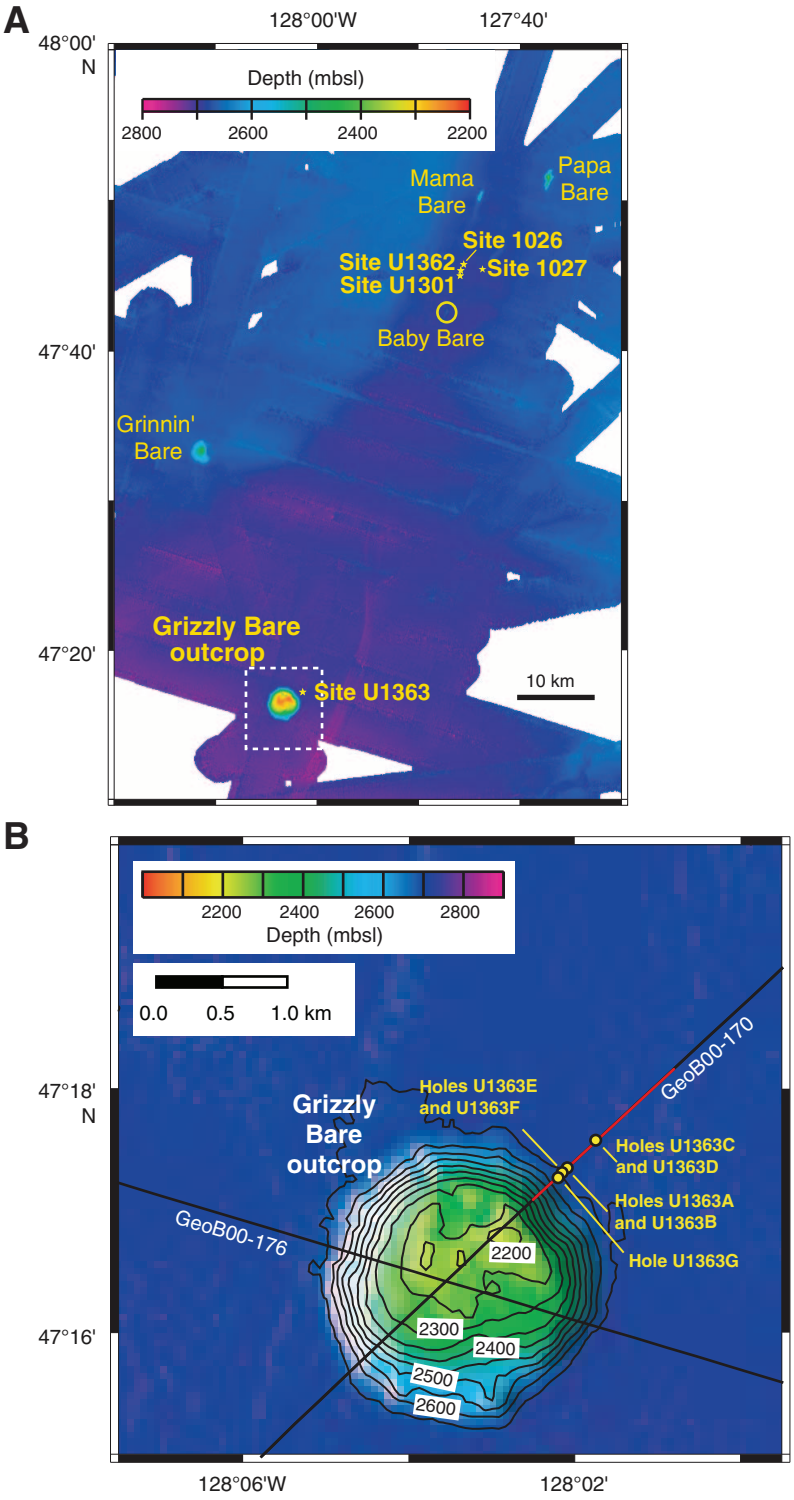

Figure F2. Seismic Line GeoB00-170 across Holes U1363A–U1363G. The sediment/basalt interface is clearly visible, but the internal structure of the Grizzly Bare edifice is not clearly imaged.

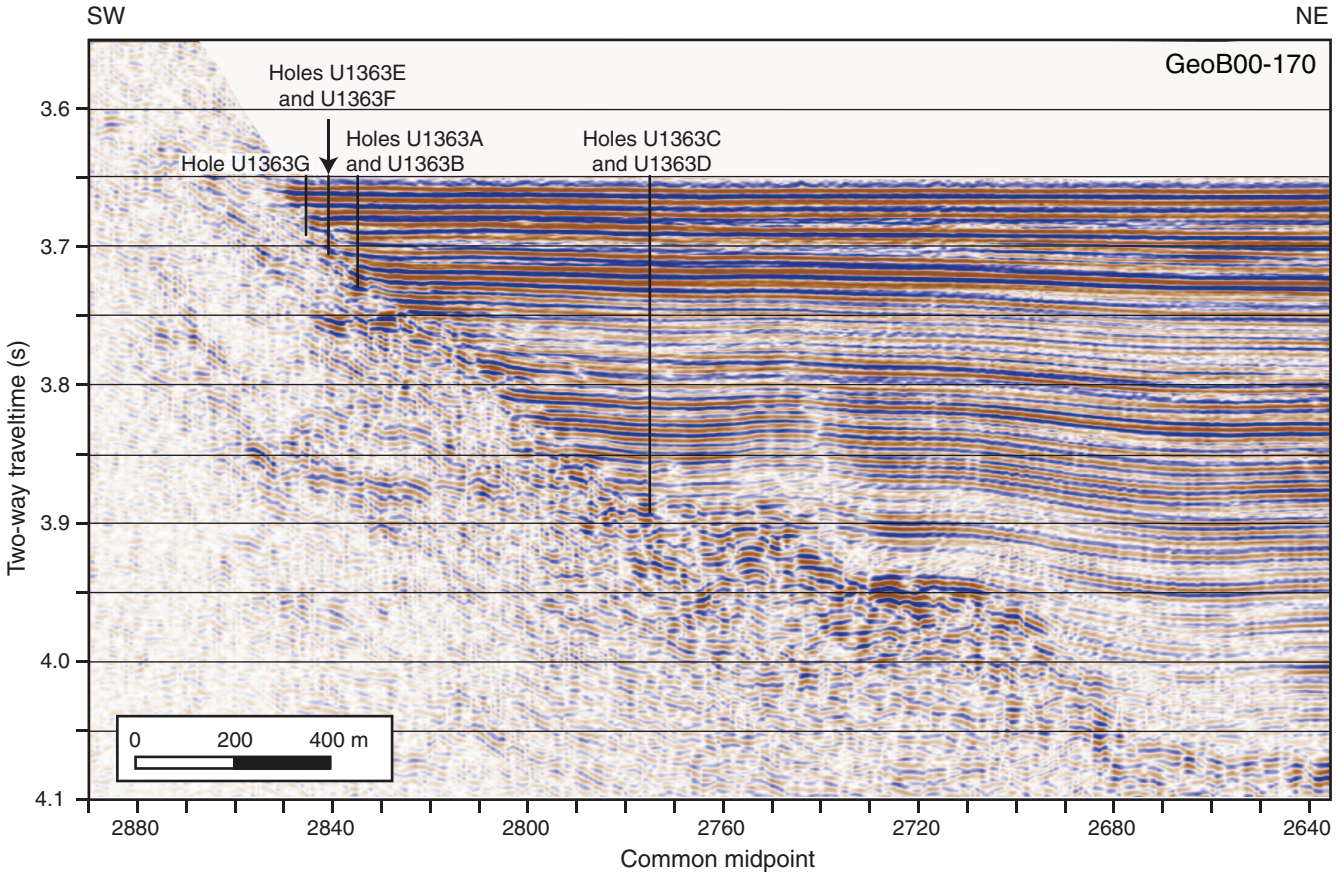

Figure F3. Lithostratigraphy, Site U1363.

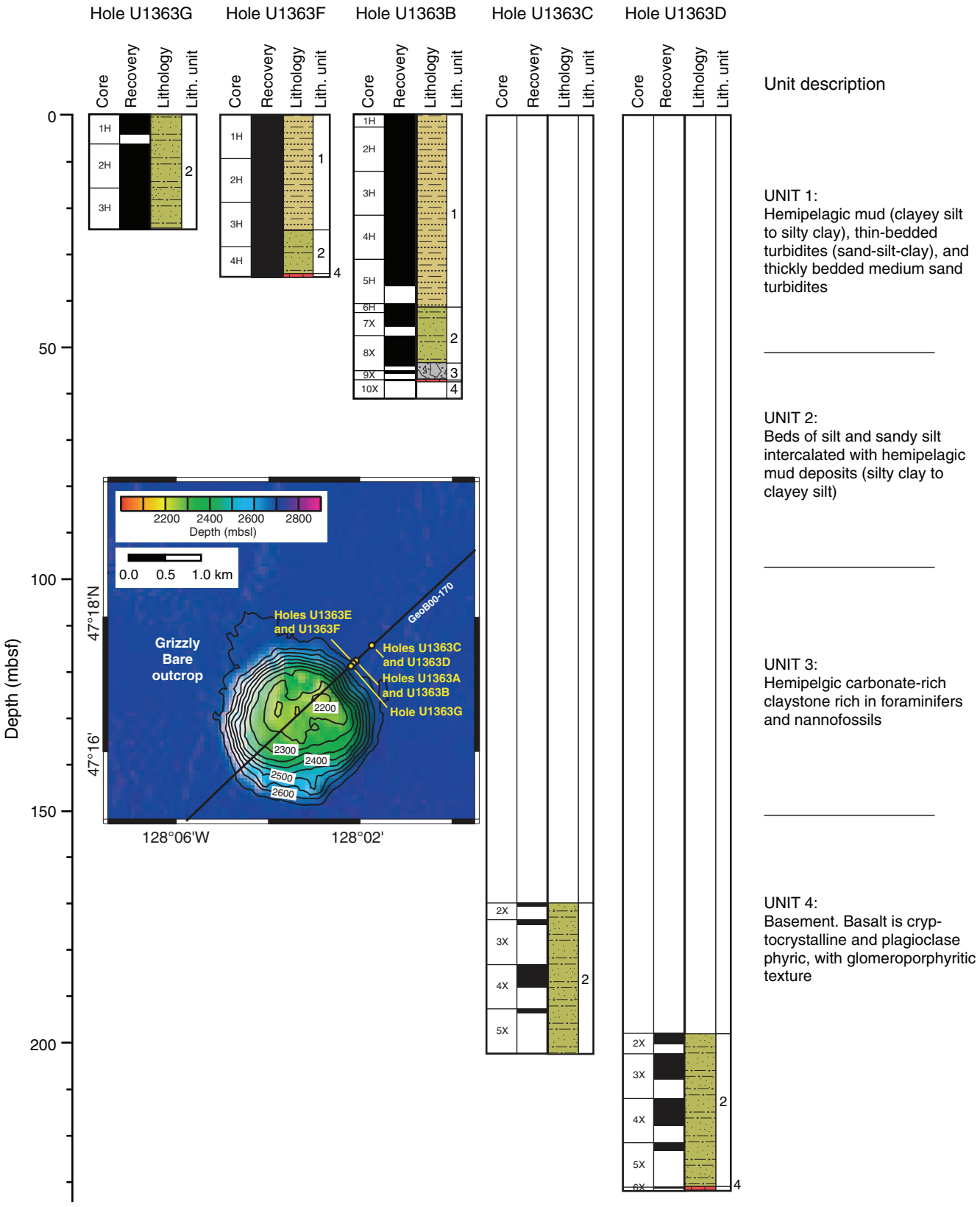

Figure F4. Pore water concentration profiles of alkalinity and pH, Site U1363. All holes were sampled to within a few meters of the sediment/basalt interface. Holes U1363C and U1363D are separated by only 10 m, so data from these sites are combined; however, only the deepest 50 m was cored (Fig. F3).

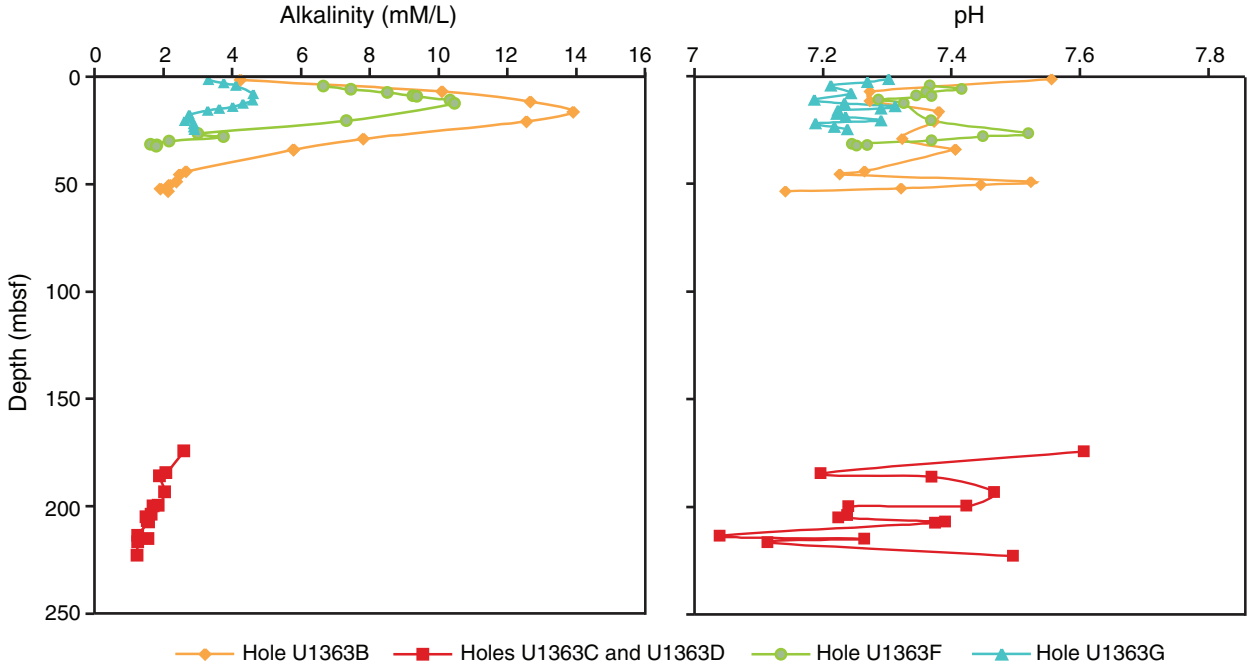

Figure F5. Plots of Site U1363 physical properties. **A.** Magnetic susceptibility from the Section Half Multisensor Logger (SHMSL) and the Whole-Round Multisensor Logger (WRMSL). **B.** Gamma ray attenuation (GRA) and moisture and density (MAD) bulk densities. Variability in MAD data is due to sample bias toward lithologic end-members. MAD bulk densities are abnormally low. **C.** MAD grain density. Hole letters are indicated by the legend suffixes.

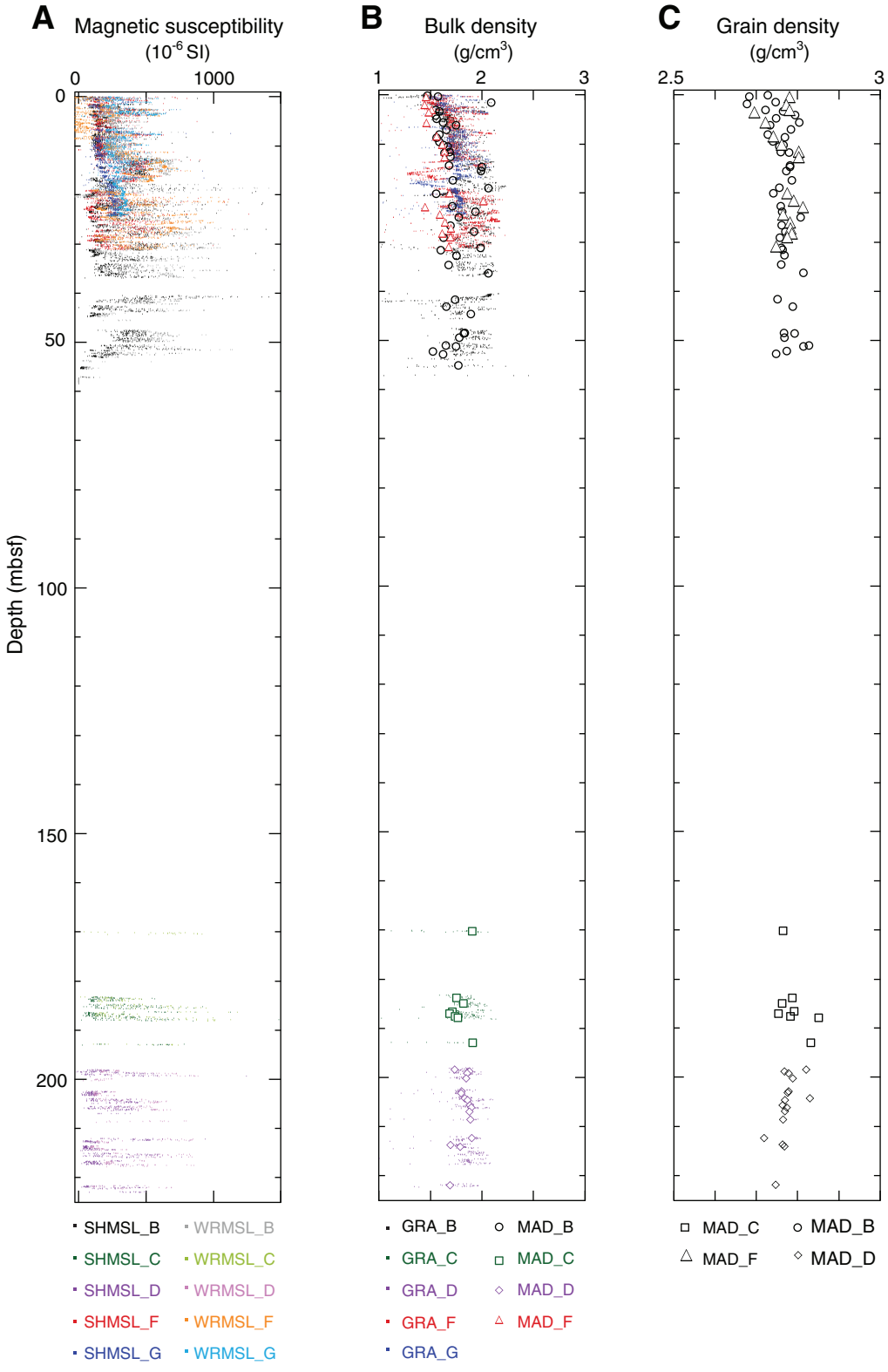

Figure F6. Plots of Site U1363 physical properties. **A.** *P*-wave velocity measured with the *P*-wave logger (PWL) and *P*-wave bayonets (along the *z*- and *y*-axes). Hole letters are indicated by the legend suffixes. **B.** Thermal conductivity. Bimodal trends are due to lithologic differences. **C.** Porosity. Bimodal trends are due to lithologic differences.

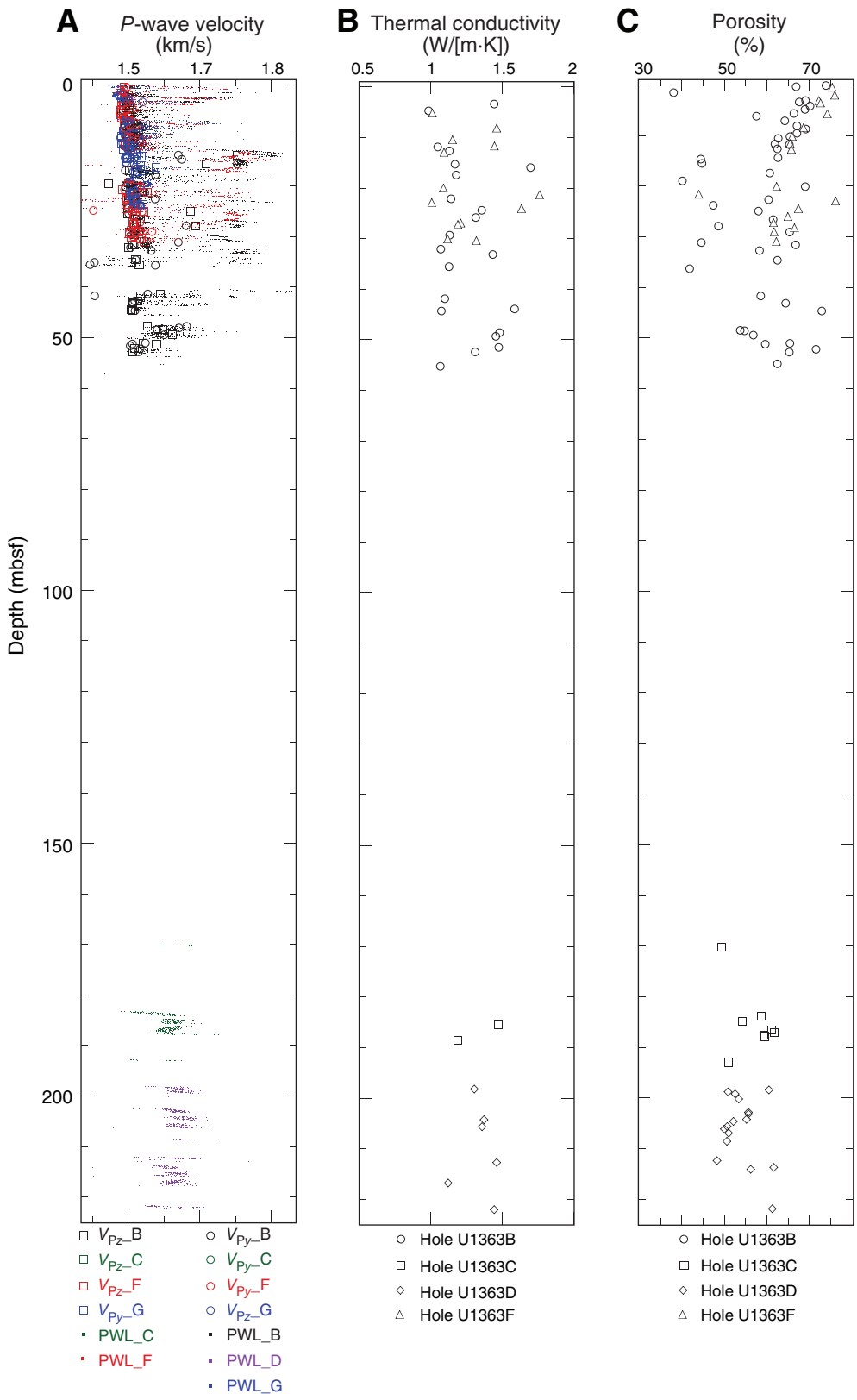

Figure F7. Cross-plots of (**A**) thermal conductivity vs. porosity and (**B**) bulk density vs. porosity, Site U1363.

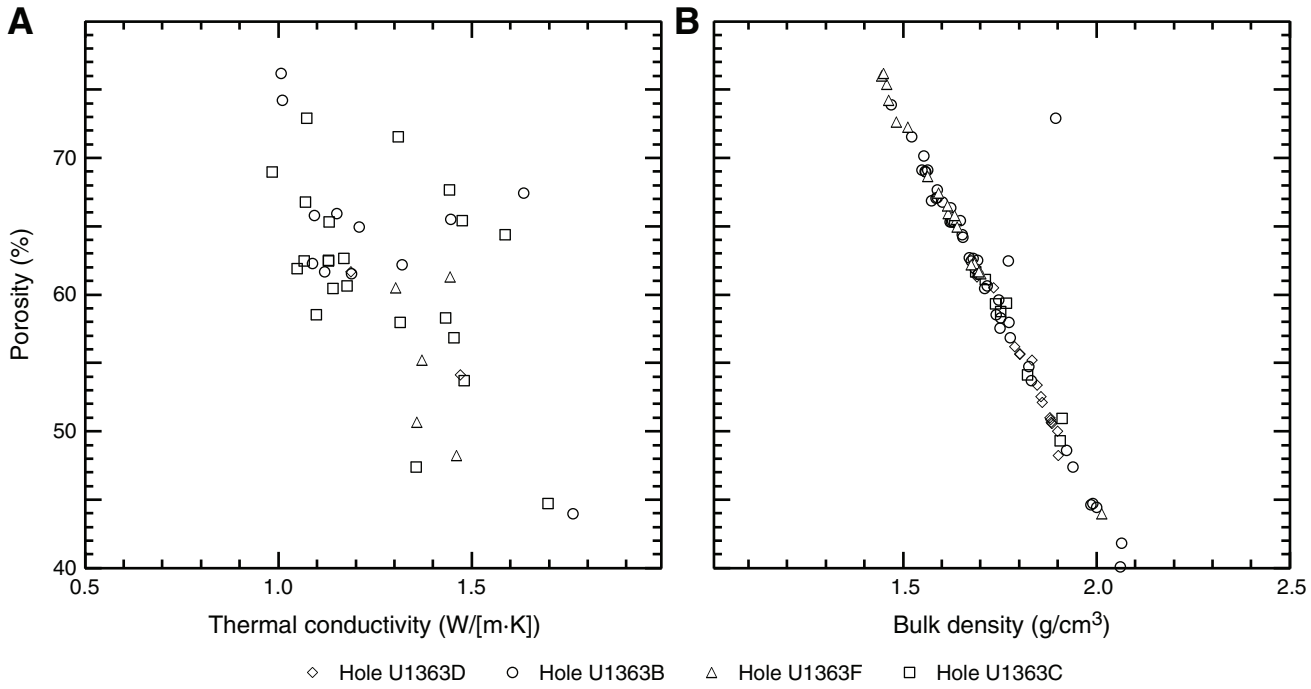

Figure F8. Cross-plot of horizontal and vertical *P*-wave velocities, Site U1363.

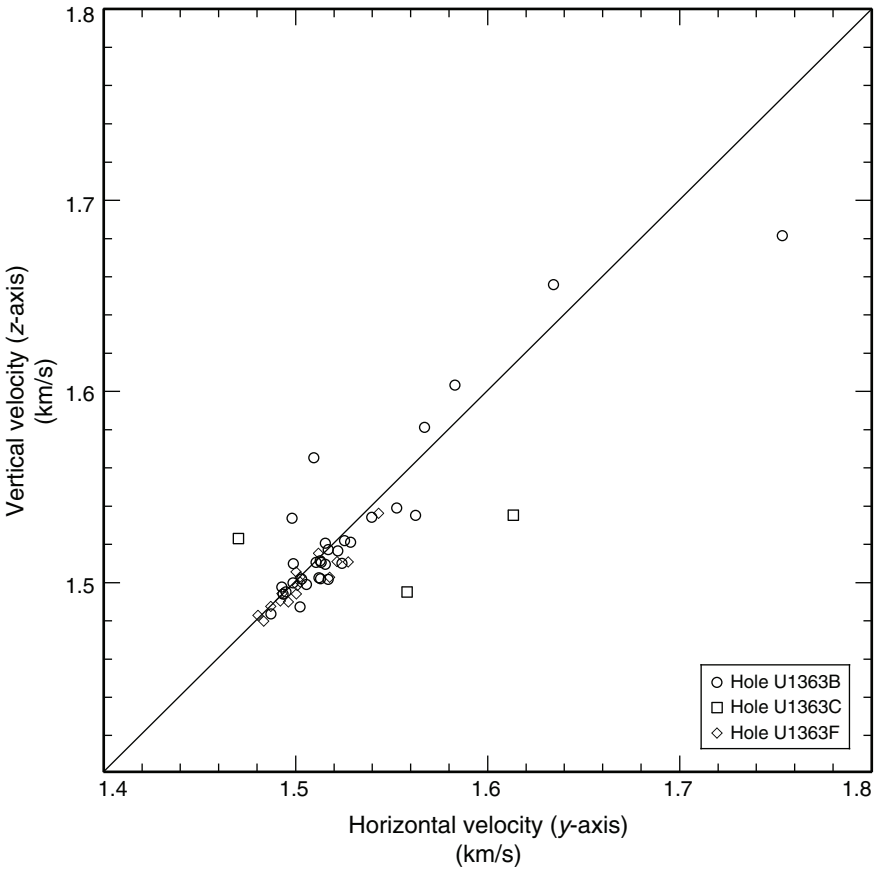

Figure F9. Cross-plots of (**A**) *P*-wave velocity vs. bulk density and (**B**) *P*-wave velocity vs. porosity, Site U1363.

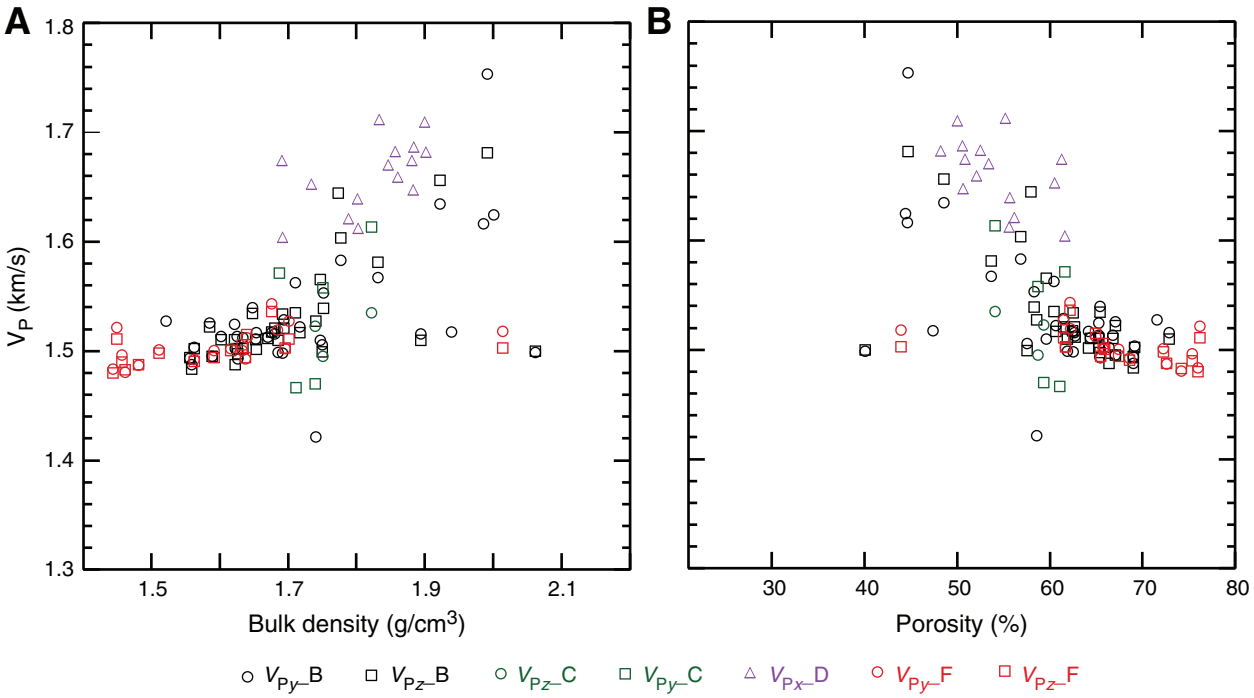

Figure F10. Plots of natural remanent magnetization intensity and inclination values obtained at 40 mT demagnetization vs. depth, Hole U1363B.

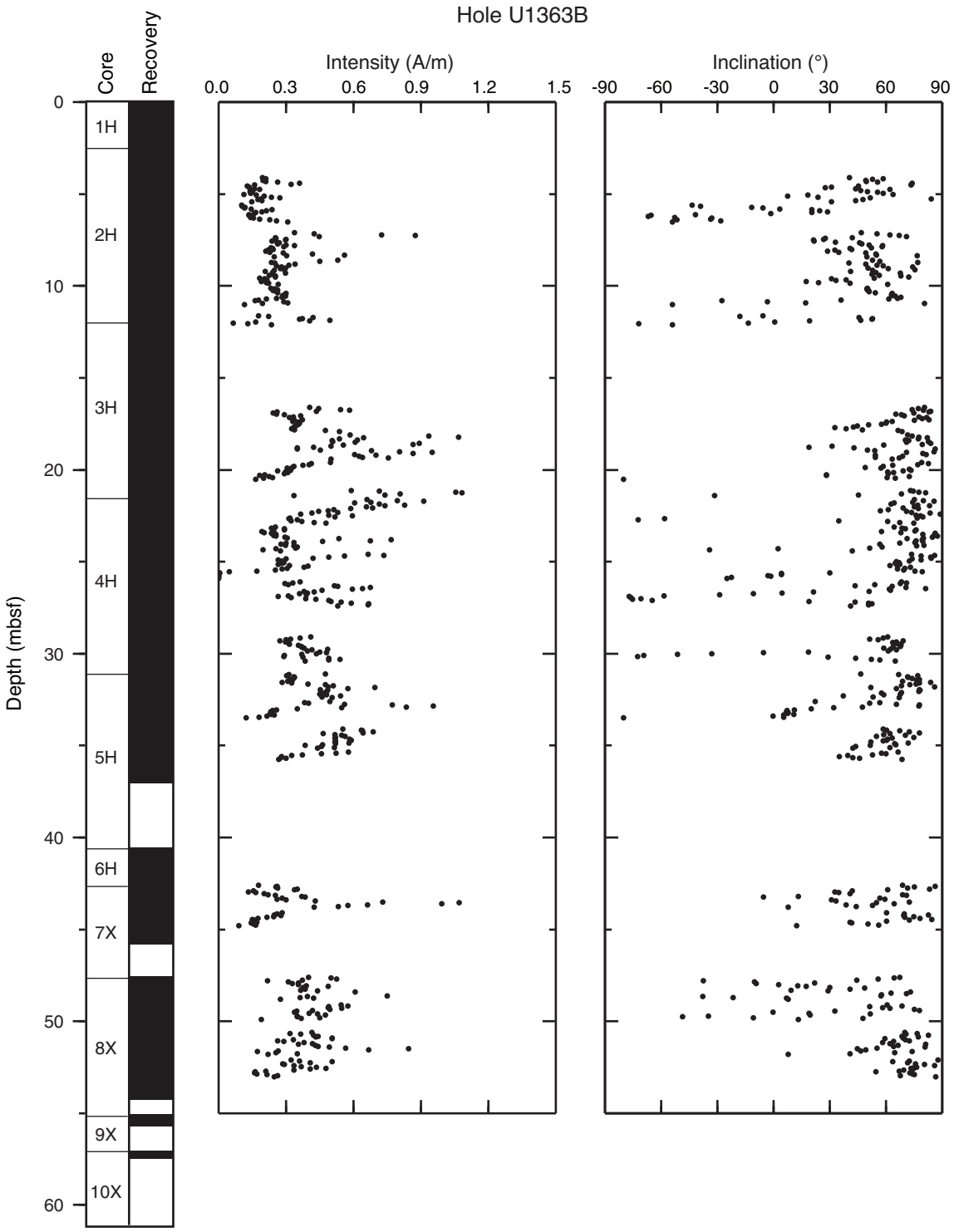

Figure F11. Plots of temperature vs. time after penetration recorded by the APCT-3 tool during deployment for Cores 327-U1363B-3H and 5H.

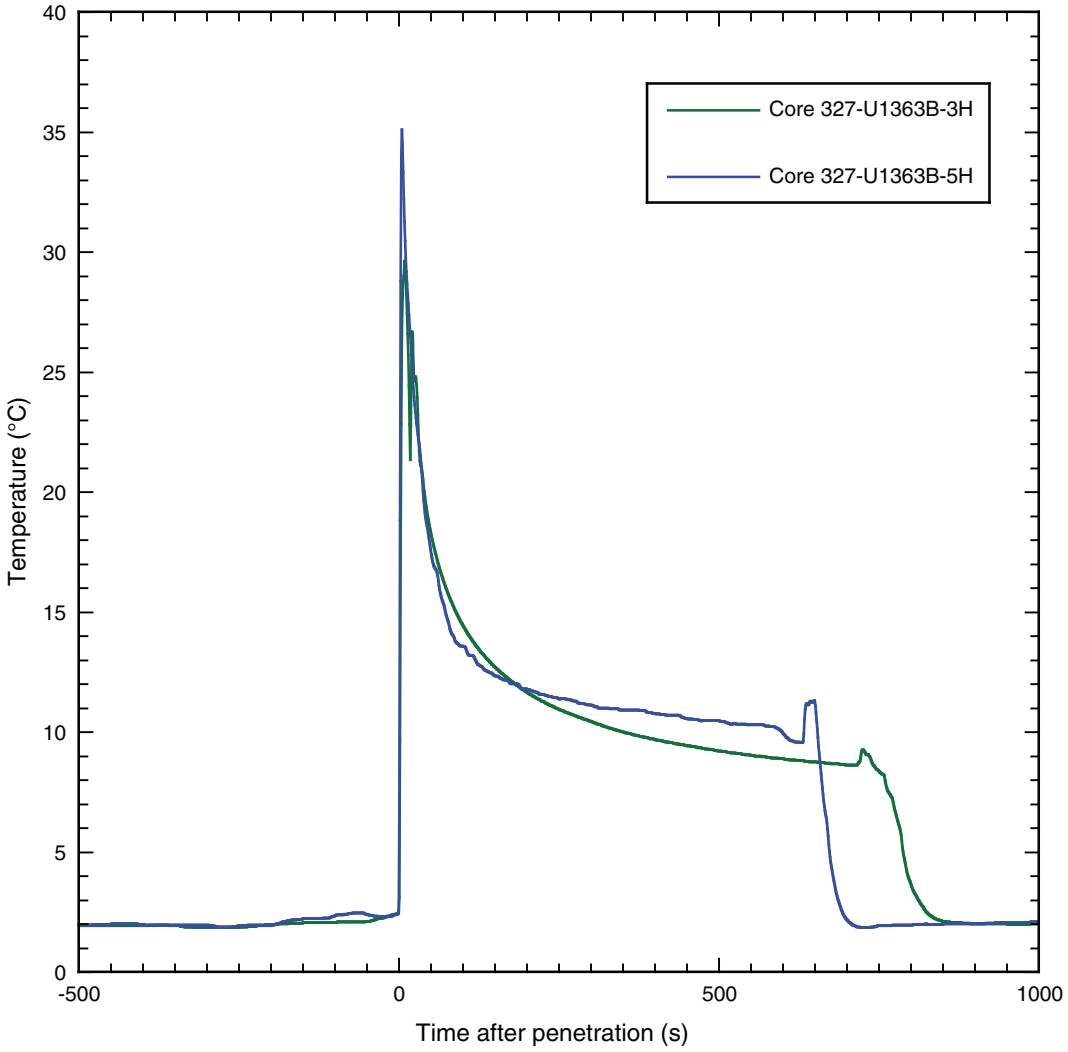

Figure F12. Plots of temperature vs. time after penetration recorded by the APCT-3 tool during deployment for Cores 327-U1363B-4H and 6H.

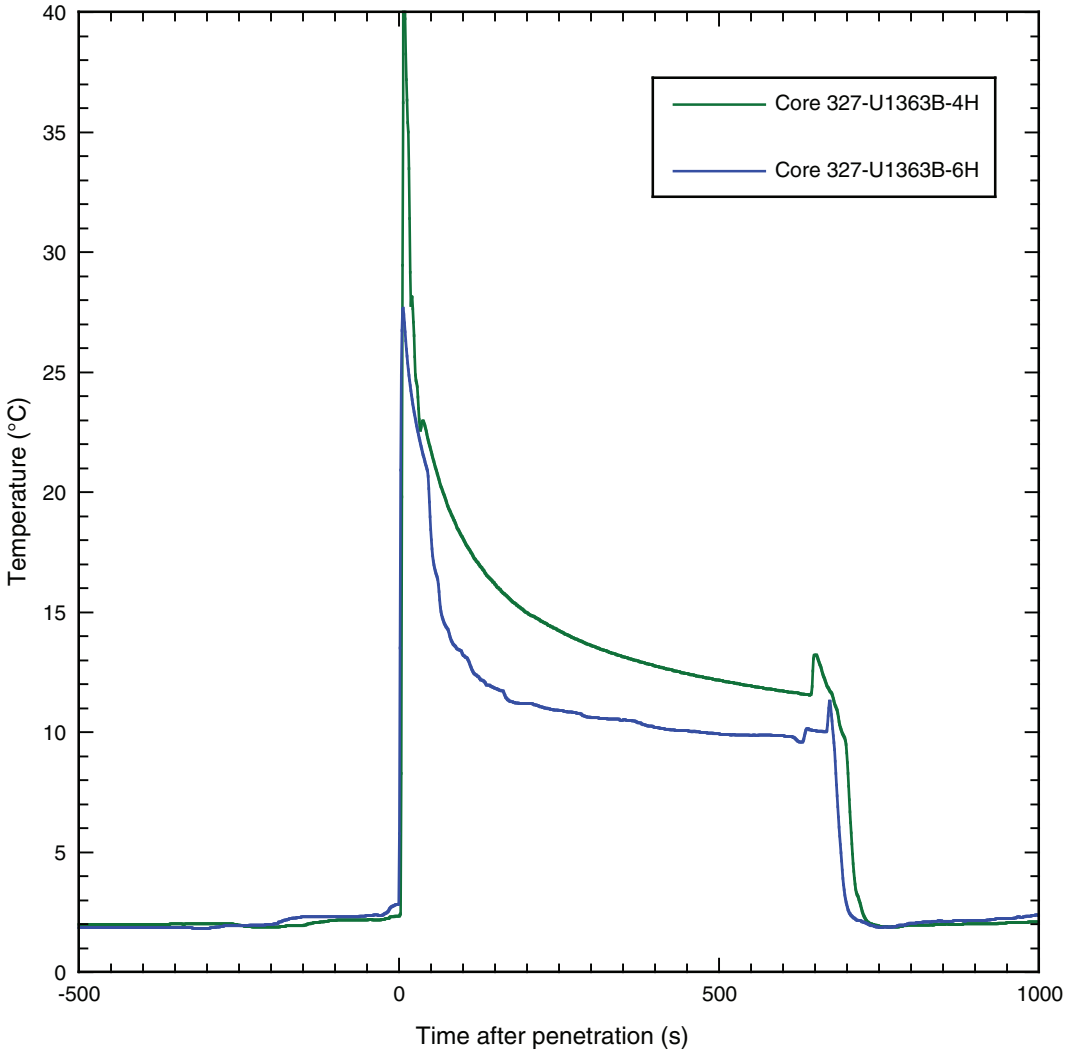

Figure F13. Plots of temperature vs. time after penetration recorded by SET tool runs after Core 327-U1363B-8X and before Core 327-U1363C-2X.

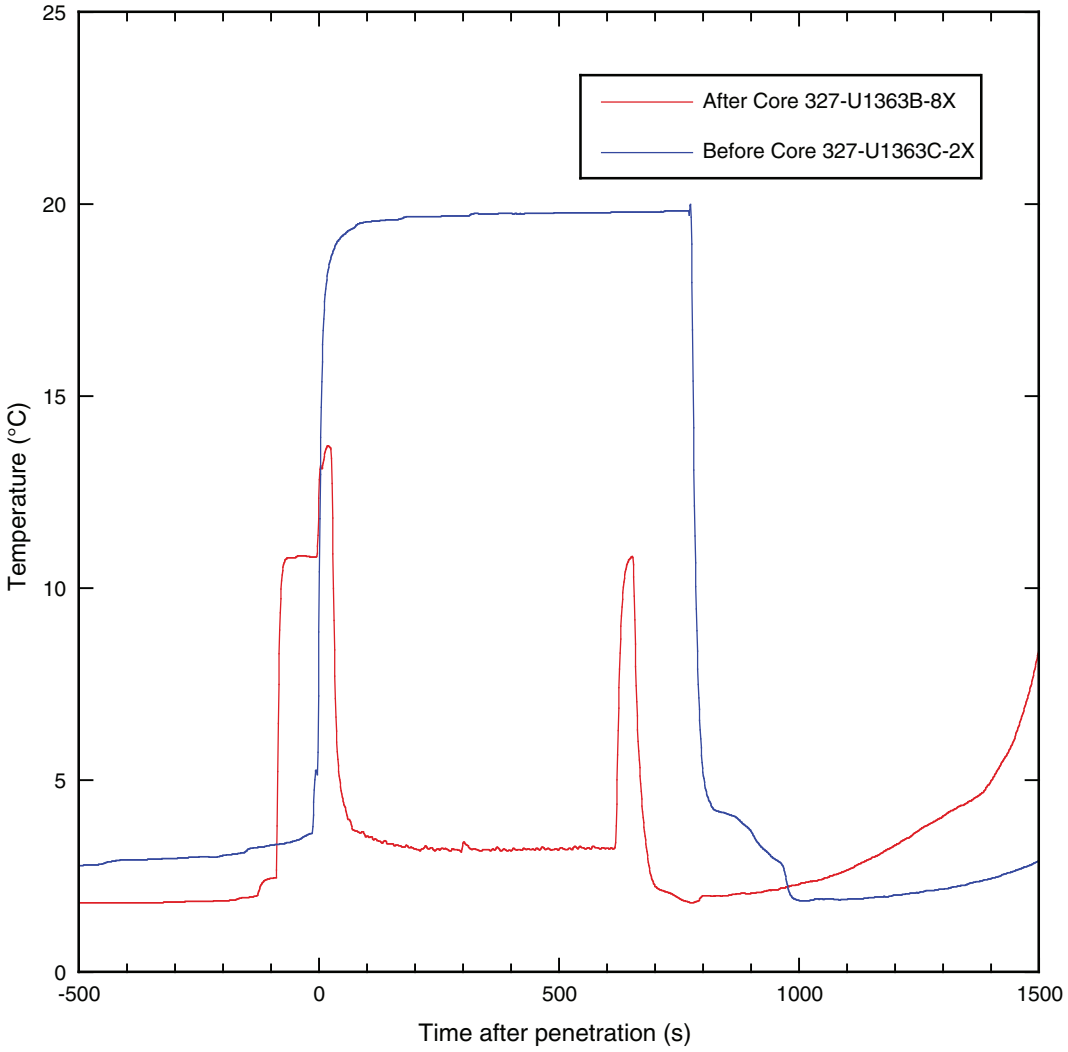

Figure F14. Plots of temperature vs. time after penetration recorded by SET tool runs after Cores 327-U1363C-3X and 5X.

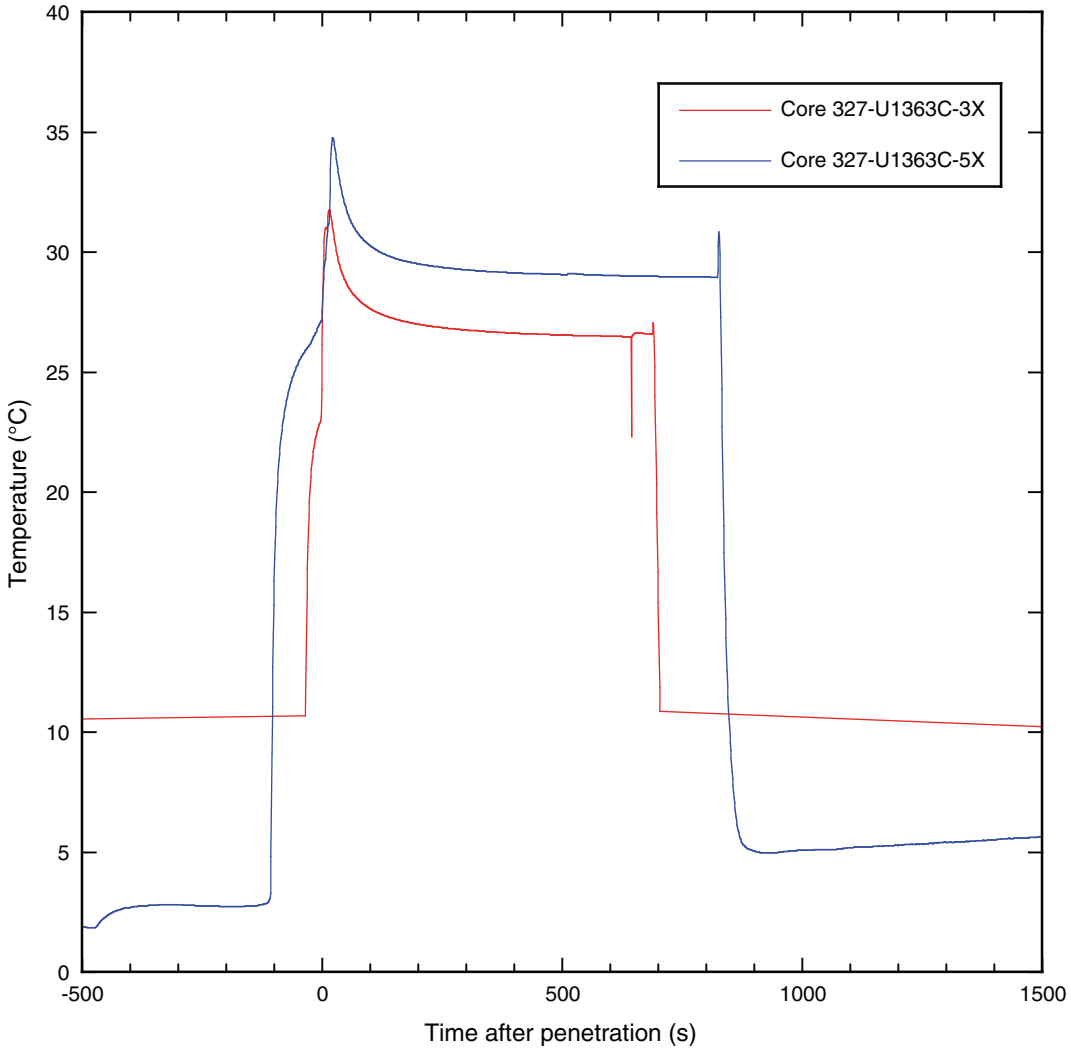

Figure F15. Plots of temperature vs. time after penetration recorded by the APCT-3 during deployment for Cores 327-U1363F-3H and 4H and 327-U1363G-2H.

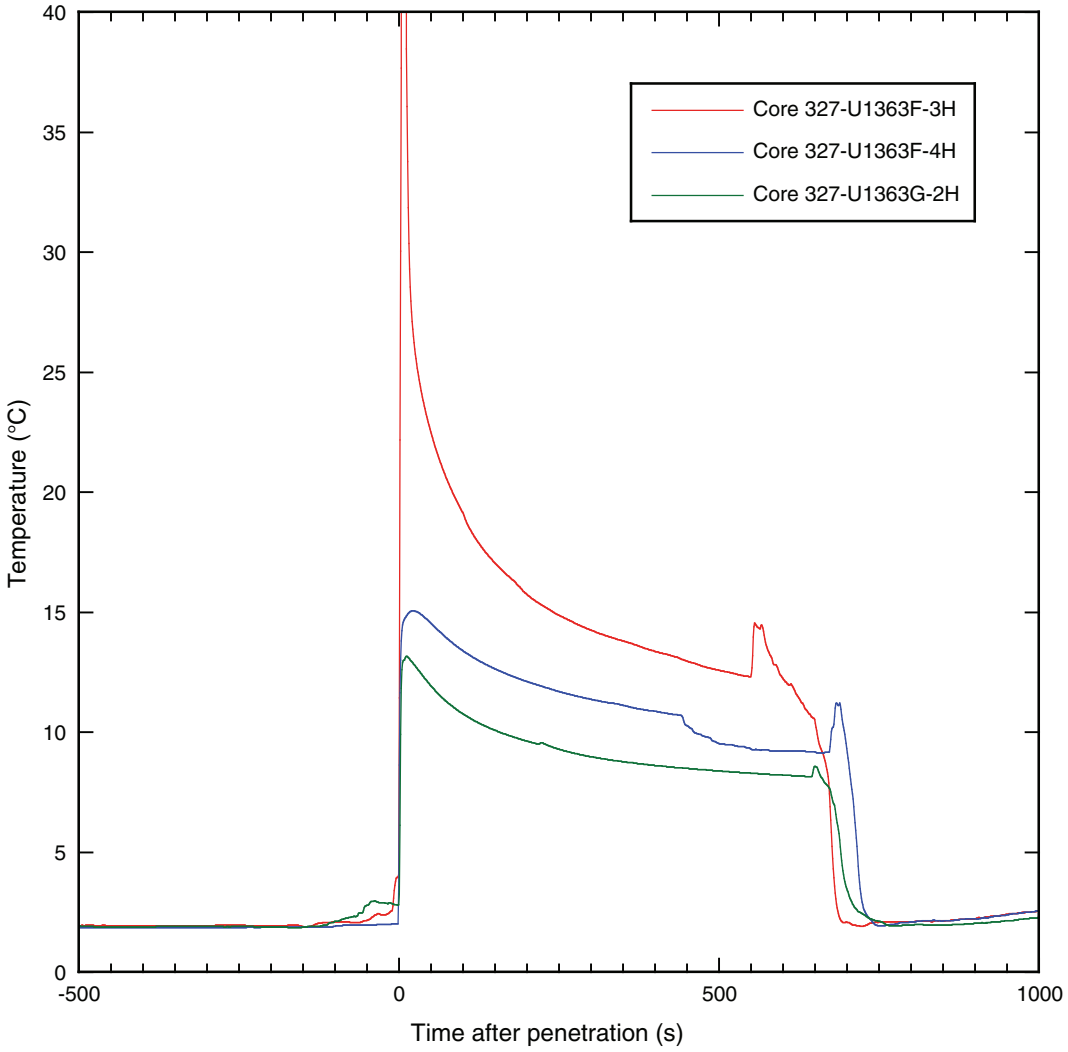

Table T1. Coring summary, Site U1363. (See table notes.) (Continued on next page.)

Hole U1363A
Latitude: 47°17.3555′N
Longitude: 128°2.1107′W
Time on hole (h): 11.25 (0.5 days)
Seafloor (drill pipe measurement from rig floor, m DRF): 2689
Distance between rig floor and sea level (m): 11.3
Water depth (drill pipe measurement from sea level, m): 2677.6
Total penetration (drilling depth below seafloor, m DSF): 58.0
Total length of cored section (m): 0
Total core recovered (m): 0
Core recovery (%): 0
Total number of cores: 0

Hole U1363B
Latitude: 47°17.3518′N
Longitude: 128°2.1060′W
Time on hole (h): 18.25 (0.8 days)
Seafloor (drill pipe measurement from rig floor, m DRF): 2690
Distance between rig floor and sea level (m): 11.3
Water depth (drill pipe measurement from sea level, m): 2678.6
Total penetration (drilling depth below seafloor, m DSF): 61.0
Total length of cored section (m): 61.0
Total core recovered (m): 49.74
Core recovery (%): 82
Total number of cores: 10

Hole U1363C
Latitude: 47°17.5759′N
Longitude: 128°1.7641′W
Time on hole (h): 27.25 (1.1 days)
Seafloor (drill pipe measurement from rig floor, m DRF): 2689
Distance between rig floor and sea level (m): 11.3
Water depth (drill pipe measurement from sea level, m): 2677.6
Total penetration (drilling depth below seafloor, m DSF): 202.4
Total length of cored section (m): 32.4
Total core recovered (m): 7.0
Core recovery (%): 22
Total number of cores: 4

Hole U1363D
Latitude: 47°17.5724′N
Longitude: 128°1.7599′W
Time on hole (h): 30 (1.3 days)
Seafloor (drill pipe measurement from rig floor, m DRF): 2689
Distance between rig floor and sea level (m): 11.3
Water depth (drill pipe measurement from sea level, m): 2677.6
Total penetration (drilling depth below seafloor, m DSF): 231.8
Total length of cored section (m): 33.8
Total core recovered (m): 15.0
Core recovery (%): 44
Total number of cores: 5

Hole U1363E
Latitude: 47°17.3310′N
Longitude: 128°2.1447′W
Time on hole (h): 4.5 (0.2 days)
Seafloor (drill pipe measurement from rig floor, m DRF): 2689
Distance between rig floor and sea level (m): 11.3
Water depth (drill pipe measurement from sea level, m): 2677.6
Total penetration (drilling depth below seafloor, m DSF): 37.0
Total length of cored section (m): 0
Total core recovered (m): 0
Core recovery (%): 0
Total number of cores: 0

Hole U1363F
Latitude: 47°17.3261′N
Longitude: 128°2.1374′W
Time on hole (h): 6 (0.3 days)
Seafloor (drill pipe measurement from rig floor, m DRF): 2689
Distance between rig floor and sea level (m): 11.3
Water depth (drill pipe measurement from sea level, m): 2677.6
Total penetration (drilling depth below seafloor, m DSF): 35.0
Total length of cored section (m): 35.0

Table T1 (continued).

Total core recovered (m): 31.2
Core recovery (%): 89
Total number of cores: 4

Hole U1363G
Latitude: 47°17.3118′N
Longitude: 128°2.1698′W
Time on hole (h): 16.75 (0.7 days)
Seafloor (drill pipe measurement from rig floor, m DRF): 2688
Distance between rig floor and sea level (m): 11.3
Water depth (drill pipe measurement from sea level, m): 2676.6
Total penetration (drilling depth below seafloor, m DSF): 24.9
Total length of cored section (m): 24.9
Total core recovered (m): 22.9
Core recovery (%): 92
Total number of cores: 3

Core	Date (2010)	Time (UTC)	Depth DSF (m) Top of cored interval	Depth DSF (m) Bottom of cored interval	Interval advanced (m)	Length of core recovered (m)	Recovery (%)	Comments
327-U1363A-								
11	31 Aug	0840	***** Drilled from 0.0 to 58.0 m DSF *****					Drilled to establish basement depth
			Hole U1363A totals:		58.0	0	0	
327-U1363B-								
1H	31 Aug	1250	0	2.5	2.5	2.5	100	
2H	31 Aug	1405	2.5	12	9.5	9.85	104	
3H	31 Aug	1535	12	21.5	9.5	9.57	101	APCT-3 deployment
4H	31 Aug	1705	21.5	31	9.5	9.95	105	APCT-3 deployment
5H	31 Aug	1830	31	40.5	9.5	5.86	62	APCT-3 deployment
6H	31 Aug	2000	40.5	42.5	2	1.76	88	APCT-3 deployment
7X	31 Aug	2150	42.5	47.5	5	3.13	63	
8X	31 Aug	2310	47.5	55	7.5	6.49	87	SET deployment
9X	1 Sep	0200	55	57	2	0.47	24	
10X	1 Sep	0400	57	61	4	0.16	4	
			Hole U1363B totals:		61.0	49.7	82	
327-U1363C-								
11	1 Sep	1333	***** Drilled from 0.0 to 170.0 m DSF *****					
2X	1 Sep	1530	170	173.6	3.6	0.5	14	SET deployment at ~171 mbsf
3X	1 Sep	1650	173.6	183.2	9.6	0.87	9	
4X	1 Sep	1925	183.2	192.8	9.6	4.9	51	SET deployment at ~184 mbsf
5X	1 Sep	2040	192.8	202.4	9.6	0.73	8	SET deployment at ~204 mbsf
			Hole U1363C totals:		202.4	7.0	22	
327-U1363D-								
11	2 Sep	2232	***** Drilled from 0.0 to 198.0 m DSF *****					
2X	2 Sep	2300	198	202.4	4.4	2.27	52	
3X	3 Sep	0235	202.4	212	9.6	5.44	57	
4X	3 Sep	0500	212	221.6	9.6	5.77	60	
5X	3 Sep	0725	221.6	231.2	9.6	1.45	15	
6X	3 Sep	0905	231.2	231.8	0.6	0.1	17	
			Hole U1363D totals:		231.8	15.0	44	
327-U1363E-								
11	3 Sep	1720	***** Drilled from 0.0 to 37.0 m DSF *****					Drilled to establish basement depth
			Hole U1363E totals:		37.0	0	0	
327-U1363F-								
1H	3 Sep	1930	0	9.5	9.5	9.54	100	
2H	3 Sep	2040	9.5	19	9.5	7.96	84	
3H	3 Sep	2200	19	28.5	9.5	9.79	103	APCT-3 deployment
4H	3 Sep	2300	28.5	35	6.5	3.89	60	APCT-3 deployment
			Hole U1363F totals:		35.0	31.18	89	
327-U1363G-								
1H	4 Sep	0320	0	6.5	6.5	4.38	67	
2H	4 Sep	0435	6.5	16	9.5	9.65	102	APCT-3 deployment
3H	4 Sep	0530	16	24.9	8.9	8.89	100	Basement at ~17 m; flow-in material
			Hole U1363G totals:		24.9	22.92	92	

Notes: DRF = drilling depth below rig floor, DSF = drilling depth below seafloor. UTC = Universal Time Coordinated. H = advanced piston corer core, X = extended core barrel core, numeric core type = drilled interval. APCT-3 = third-generation advanced piston corer temperature tool, SET = Sediment Temperature tool.

Table T2. Depth summary, Site U1363. (See table note.)

Hole	Depth to basement mbrf	Depth to basement mbsf	Comments
327-			
U1363A	2747.0	58.0	Tagged basement when drilling
U1363B	2748.0	57.0	Basement contact in Core 327-U1363B-9X
U1363C	NA	NA	Hole terminated when SET stuck
U1363D	2920.2	231.2	Basement contact in Core 327-U1363D-5X
U1363E	2725.0	36.0	Tagged basement when drilling
U1363F	2724.0	35.0	Manganese crust in Core 327-U1363F-4H
U1363G	2705.0	17.0	Tagged basement in adjacent (unnumbered) hole; most of Core 327-U1363G-3H is flow-in

Note: NA = not applicable, SET = Sediment Temperature tool.

Table T3. Pore water chemical data, Site U1363. This table is available in an oversized format.

Table T4. Shore-based pore water data for ammonium, phosphate, and nitrate plus nitrite, Site U1363.

Core, section	Depth average (m)	Ammonium color (μM)	Phosphate color (μM)	$NO_3 + NO_2$ color (μM)
327-U1363B-				
1H-1	1.2	191	13.2	1.2
2H-3	6.8	820	38.2	1.9
2H-6	11.3	1030	65.6	2.1
3H-3	16.3	911	66.0	1.7
3H-6	20.8	978	54.0	1.9
4H-3	25.8	702	18.1	1.2
4H-5	28.8	734	12.8	1.2
5H-2	33.8	565	14.2	1.2
7X-2	45.1	172	1.99	1.7
8X-2	50.2	211	3.41	1.5
8X-5	53.56	156	0.87	0.5
327-U1363C-				
3X-1	173.6	397	0.63	1.5
4X-1	184.2	383	1.93	1.2
4X-2	185.7	297	0.69	1.7
327-U1363D-				
2X-2	199.57	269	0.69	2.6
3X-1	203.35	186	0.22	3.3
3X-2	204.9	271	0.63	1.7
3X-3	206.35	205	0.51	2.6
3X-4	207.22	202	0.48	1.9
4X-2	214.5	209	0.69	3.1
5X-1	222.3	236	0.40	1.7
327-U1363F-				
1H-3	4.3	425	17.0	1.2
1H-4	5.8	422	27.8	2.6
1H-5	7.3	496	34.2	2.6
1H-6	8.8	655	50.9	2.4
1H-7	9	543	40.7	1.9
2H-1	10.8	684	23.2	2.1
2H-2	12.3	636	28.5	1.2
2H-3	13.8	769	42.9	1.7
2H-4	15.25	448	26.9	2.6
3H-1	20.3	504	16.1	2.1
3H-3	23.26	683	13.2	1.2
3H-5	26.26	432	4.86	3.0
3H-6	27.76	409	4.12	2.1
4H-1	29.65	282	2.58	2.6
4H-2	31.15	294	1.70	2.1
4H-3, upper	31.5	308	1.46	2.1
4H-3	31.94	159	1.81	2.4
327-U1363G-				
1H-1	1.3	147	13.2	1.7
1H-2	2.66	180	16.3	1.0
1H-3	3.95	482	13.4	1.9
2H-1	7.8	192	15.4	1.5
2H-2	9.3	274	11.9	1.7
2H-3	10.8	188	12.7	1.5
2H-4	12.3	196	8.61	1.5
2H-5	13.8	140	6.36	1.5
2H-6	14.8	194	6.66	1.7
2H-7	15.57	95	4.36	1.2
3H-1	17.3	138	2.88	2.6
3H-2	18.8	151	2.70	1.9
3H-3	20.3	131	3.47	2.1
3H-4	21.8	176	3.17	2.4
3H-5	23.25	722	1.81	3.1
3H-6	24.34	128	2.82	1.9

Table T5. Microsphere contamination of sediment samples, Hole U1363B.

Core, section	Depth (mbsf)	Description	Microspheres/cm^3	
			Exterior	Interior
327-U1363B-				
1H-1	0.68	Clay	0	0
2H-3	6.48	Clay	0	0
2H-6	10.98	Clay	0	0
3H-3	15.98	Sandy clay	0	0
3H-6	20.48	Clay	0	0
4H-3	25.48	Clay	0	0
4H-5	28.48	Clay	0	0
5H-2	33.48	Sandy clay	0	0
7X-2	44.78	Clay	0	0
8X-2	49.88	Clay	0	0
8X-5	53.36	Foraminifer rich	0	0

Table T6. Microsphere contamination of sediment samples, Holes U1363C and U1363D. (See table note.)

Core, section	Depth (mbsf)	Description	Microspheres/cm^3	
			Exterior	Interior
327-U1363C-				
3X-1	173.60	Clay	0	0
4X-1	184.18	Clay	0	0
4X-2	195.68	Clay	0	0
5X-1(CC)	193.03	Sandy clay	0	NA
327-U1363D-				
2X-2	199.55	Clay	0	0
3X-1	203.33	Clay	0	0
3X-2	204.88	Clay	0	0
3X-3	206.33	Sandy clay	0	0
3X-4	207.20	Clay	0	0
4X-1	212.93	Clay	0	0
4X-2	214.48	Clay	5.3×10^2	0
4X-3	215.93	Sandy clay	0	0
5X-1	228.28	Clay	2.6×10^4	5.8×10^3

Note: NA = not applicable.

Table T7. Microsphere contamination of sediment samples, Hole U1363F. (See table note.)

Core, section	Depth (mbsf)	Description	Microspheres/cm^3	
			Exterior	Interior
327-U1363F-				
1H-3	4.28	Clay	2.2×10^4	5.6×10^2
1H-4	5.78	Clay	1.1×10^4	0
1H-5	7.28	Clay	0	0
1H-6	8.78	Clay	0	0
2H-1	10.78	Clay	0	0
2H-2	12.28	Sandy clay	1.3×10^3	0
2H-3	13.78	Sandy clay	4.0×10^3	5.3×10^2
2H-4	15.23	Sandy clay	4.4×10^2	0
3H-1	20.28	Clay	6.7×10^4	0
3H-3	23.24	Clay	0	8.0×10^2
3H-5	26.74	Sandy clay	0	0
3H-6	27.74	Sandy clay	0	0
4H-1	29.63	Clay	0	0
4H-2	31.13	Clay and Mn crust	0	0
4H-3	31.92	Clay and Mn crust, foraminifer rich	0	0
4H-CC	32.34	Mn crust and basalt sand	1.3×10^4	NA

Note: NA = not applicable.

Table T8. Microsphere contamination of sediment samples, Hole U1363G.

Core, section	Depth (mbsf)	Description	Microspheres/cm^3	
			Exterior	Interior
327-U1363G-				
1H-1	1.28	Sandy clay	5.0×10^2	0
1H-2	2.64	Sandy clay	5.7×10^3	0
1H-3	3.93	Clay	0	0
2H-1	7.78	Clay	0	0
2H-2	9.28	Clay	0	0
2H-3	10.78	Clay	0	0
2H-4	12.28	Clay	0	0
2H-5	13.78	Clay	0	0
2H-6	14.78	Clay	0	0
2H-7	15.55	Clay	0	0
3H-1	17.28	Clay	1.6×10^5	4.7×10^3
3H-2	18.78	Clay	1.3×10^3	0
3H-3	20.23	Clay	8.0×10^4	0
3H-4	21.78	Clay	1.5×10^3	0
3H-5	23.23	Clay	0	0
3H-6	24.32	Clay	0	0

Table T9. Physical property data, Site U1363. (See table note.) (Continued on next page.)

Core, section, interval (cm)	Top depth (mbsf)	Bulk density (g/cm^3)	Grain density (g/cm^3)	Porosity (vol%)	V_{P_x} (m/s)	V_{P_y} (m/s)	V_{P_z} (m/s)	Thermal conductivity (W/[m·K])
327-U1363B-								
1H-1W, 15–17	0.15	1.47	2.73	73.91				
1H-1W, 39–41	0.39	1.57	2.68	66.89				
1H-2W, 3–5	1.53	2.09	2.75	38.06				
2H-1W, 60–62	3.10	1.55	2.72	69.11				
2H-1W, 90–92	3.40	1.59	2.76	67.64				1.44
2H-2W, 20–22	4.20	1.55	2.79	70.14				
2H-2W, 84–86	4.84	1.56	2.75	68.98		1487	1484	0.98
2H-3W, 14–16	5.64	1.62	2.80	66.36		1502	1487	
2H-3W, 72–74	6.22	1.75	2.73	57.54		1506	1499	
2H-4W, 10–12	7.10	1.65	2.78	64.21		1517	1502	
2H-4W, 110–112	8.10	1.59	2.73	67.06		1526	1522	
2H-5W, 20–22	8.70	1.56	2.77	69.13		1503	1502	
2H-5W, 105–107	9.55	1.59	2.74	67.08		1495	1495	
2H-6W, 24–26	10.24	1.63	2.77	65.39		1493	1498	
2H-6W, 58–60	10.58	1.67	2.76	62.70		1513	1512	
2H-7W, 20–22	11.70	1.69	2.76	61.88		1499	1510	1.05
2H-7W, 30–32	11.80	1.63	2.78	65.27		1512	1503	
3H-1W, 65–67	12.65	1.69	2.80	62.49		1498	1534	1.13
3H-2W, 90–92	14.40	1.68	2.78	62.63		1516	1521	1.17
3H-2W, 116–118	14.66	2.00	2.78	44.42		1625		
3H-3W, 50–52	15.50	1.99	2.77	44.70		1754	1682	1.70
3H-4W, 94–96	17.44	1.72	2.79	60.66		1522	1517	1.18
3H-5W, 96–98	18.96	2.06	2.76	40.10		1499	1500	
3H-6W, 60–62	20.10	1.56	2.74	69.00		1494	1494	
4H-1W, 118–120	22.68	1.71	2.76	60.44		1563	1535	1.14
4H-2W, 80–82	23.80	1.94	2.76	47.40		1517		1.36
4H-3W, 44–46	24.94	1.77	2.81	57.99			1644	1.31
4H-4W, 58–60	26.58	1.69	2.76	61.47		1529	1521	
4H-5W, 38–40	27.88	1.92	2.77	48.59		1635	1656	
4H-6W, 7–9	29.07	1.63	2.76	65.31		1513	1502	1.13
4H-7W, 64–66	31.14	1.99	2.76	44.61		1616		
5H-1W, 62–64	31.62	1.60	2.76	66.77		1513	1511	1.07
5H-2W, 24–26	32.74	1.75	2.77	58.27		1553	1539	1.43
5H-3W, 61–63	34.61	1.68	2.76	62.47		1518	1517	1.13
5H-5W, 43–45	36.29	2.07	2.81	41.83				
6H-2W, 21–23	41.71	1.74	2.75	58.55			1528	1.10
7X-1W, 62–64	43.12	1.65	2.79	64.40		1511	1511	1.59
7X-2W, 65–67	44.65	1.89				1516	1510	1.07
8X-1W, 94–97	48.44	1.83	2.77	53.71		1567	1581	1.48
8X-1W, 106–108	48.56	1.82	2.79	54.73				
8X-2W, 40–42	49.40	1.78	2.77	56.83		1583	1603	1.46

Table T9 (continued).

Core, section, interval (cm)	Top depth (mbsf)	Bulk density (g/cm^3)	Grain density (g/cm^3)	Porosity (vol%)	V_{P_x} (m/s)	V_{P_y} (m/s)	V_{P_z} (m/s)	Thermal conductivity (W/[m·K])
8X-3W, 54–56	51.04	1.65	2.83	65.42		1540	1534	1.48
8X-3W, 71–73	51.21	1.75	2.81	59.60		1510	1566	
8X-4W, 22–24	52.22	1.52	2.77	71.55		1527		1.31
8X-4W, 79–81	52.79	1.62	2.75	65.30		1524	1510	
9X-1W, 8–10	55.08	1.77	3.02	62.46				1.07
327-U1363C-								
2X-CCW, 20–22	170.20	1.91	2.76	49.29	1672			
4X-1W, 65–67	183.85	1.75	2.79	58.75		1558	1496	
4X-2W, 24–26	184.94	1.82	2.76	54.12		1613	1535	1.47
4X-3W, 38–40	186.58	1.71	2.79	61.09		1466		
4X-3W, 81–83	187.01	1.69	2.75	61.65		1571		1.19
4X-3W, 138–140	187.58	1.74	2.78	59.33		1470	1523	
4X-CCW, 18–20	187.88	1.77	2.85	59.38				
5X-1W, 17–19	192.97	1.91	2.83	50.95				
327-U1363D-								
2X-1W, 41–43	198.41	1.73	2.82	60.50	1653			1.30
2X-1W, 78–80	198.78	1.88	2.77	50.87	1674			
2X-1W, 120–122	199.20	1.86	2.78	52.52	1682			
2X-CC	200.18	1.85	2.79	53.39	1670			
3X-1W, 42–44	202.82	1.80	2.78	55.64	1612			
3X-1W, 74–76	203.14	1.80	2.78	55.67	1639			
3X-2W, 34–36	204.24	1.83	2.83	55.20	1712			1.37
3X-2W, 73–75	204.63	1.86	2.77	52.11	1659			
3X-3W, 26–28	205.66	1.88	2.76	50.64	1648			1.36
3X-3W, 75–77	206.15	1.90	2.77	49.99	1709			
3X-4W, 4–6	206.94	1.88	2.77	50.99				
3X-CCW, 17–19	208.57	1.88	2.76	50.58	1687			
4X-1W, 36–38	212.36	1.90	2.72	48.24	1682			1.46
4X-2W, 22–24	213.72	1.69	2.76	61.60	1604			
4X-2W, 61–63	214.11	1.79	2.77	56.18	1621			
4X-4W	216.80							1.12
5X-1W, 31–33	221.91	1.69	2.75	61.30	1674			1.44
327-U1363F-								
1H-1W, 51–53	0.51	1.46	2.78	75.36		1496	1490	
1H-2W, 53–55	2.03	1.44	2.77	75.99		1484	1480	
1H-3W, 10–12	3.10	1.51	2.78	72.25		1501	1498	
1H-3W, 55–57	3.55	1.48	2.70	72.62		1487.08	1487.51	
1H-4W, 119–121	5.69	1.46	2.72	74.23		1481	1483	1.01
1H-5W	7.10							1.46
1H-6W, 96–98	8.46	1.56	2.74	68.62		1492	1491	
2H-1W, 67–69	10.17	1.62	2.76	65.92		1502	1500	1.15
2H-2W, 56–58	11.56	1.64	2.80	65.51		1493	1494	1.45
2H-3W, 21–23	12.71	1.63	2.80	65.77		1500	1506	1.09
3H-1W, 104–106	20.04	1.68	2.77	62.25	1569	1519		1.09
3H-2W, 110–112	21.60	2.01	2.79	43.96		1518	1503	1.76
3H-3W, 94–96	22.90	1.45	2.81	76.18		1522	1511	1.01
3H-4W, 98–100	24.44	1.59	2.76	67.40		1500	1494	1.63
3H-5W, 101–103	25.97	1.64	2.78	64.95		1512	1515	1.21
3H-6W, 77–79	27.23	1.70	2.78	61.51		1527	1511	1.19
3H-7W, 28–30	28.24	1.61	2.79	66.48				
4H-1W, 53–55	29.03	1.70	2.78	61.66		1502	1503	1.12
4H-2W, 93–95	30.93	1.68	2.75	62.21		1543	1536	1.32

Note: Velocity values displayed in this table were measured around the measurement points of MAD properties.